Bistatic Measurement Fusion from Multistatic Configurations for Air Collision Warning

WENBO DOU
YAAKOV BAR-SHALOM
PETER WILLETT

A requisite for unmanned aircraft systems (UAS) to operate within a controlled airspace is a capability to sense and avoid collisions with non-cooperative aircraft. Ground-based transmitters and UAS-mounted receivers are preferred due to limitations on UAS. This paper assumes a constant velocity motion of an intruder (target) aircraft and presents a method to estimate the position and velocity of the target so as to predict the closest point of approach. Bistatic range and range rate are assumed the only measurements available. Several configurations are investigated from a parameter observability point of view. It turns out that one needs three transmitters in a general three-dimensional scenario to achieve decent observability of the target motion parameter. With the assumption that the target is at the same altitude as the ownship, one has a two-dimensional scenario in which two transmitters are required in order to have good observability. Simulation results show that the maximum likelihood (ML) estimate of the target parameter using an iterated least squares search can be considered as statistically efficient in both multistatic configurations with good observability for the scenarios considered in this paper. The collision warning can be carried out based on the ML estimate in two different ways. The first approach is to formulate the collision as a hypothesis testing problem using a generalized likelihood function. A second, Bayesian, approach is also presented. The performance of the likelihood based collision warning shows that the multistatic configuration with three transmitters is reliable for collision warning but that the multistatic configuration with two transmitters under the same target and ownship altitude assumption is prone to false alarms. In the configuration with three transmitters, the Bayesian approach yields the similarly reliable collision warning performance as the likelihood-based approach when they use threshold values of the same magnitude.

Manuscript received July 28, 2015; revised October 12, 2015: released for publication November 9, 2015.

Refereeing of this contribution was handled by Benjamin Slocumb.

Supported by ARO Grant W991NF-10-1-0369.

Authors' address: Department of Electrical and Computer Engineering, University of Connecticut, Storrs, CT 06269-4157 (e-mail: {dou, ybs, willett}@engr.uconn.edu.)

1. INTRODUCTION

Sense-and-Avoid (SAA) capabilities are required for unmanned aircraft systems (UAS) to operate within the national airspace, since the proliferation of UAS has increased the risk of aircraft collision. The air traffic control radar beacon system works well to coordinate cooperative aircraft. Active sensing methods have to be employed for UAS to be functional against non-cooperative targets. The limitations on the size, weight and power of UAS suggest an implementation with ground-based transmitters and UAS-mounted receivers.

There have been numerous works on the UAS collision avoidance problem [1]. Most have emphasized avoidance algorithms [5][13][15], while sensing and estimation methods have been less extensively explored. In [9], a monostatic radar configuration in a two-dimensional (2-D) plane with range and bearing measurements is considered for collision avoidance. In [18], collision warning in a 2-D plane using a monostatic radar with range and azimuth measurements is discussed. A confidence ellipsis at a given time instant is mathematically derived and a confidence corridor is constructed by the regions covered by all confidence ellipses at all time instants within a time interval of interest. A warning decision is based on whether any target aircraft falls within this confidence corridor. The collision warning problem in a multistatic radar configuration has not yet been reported in the literature.

Target localization is possible using a multistatic radar with time of arrival (TOA) measurements [6][10][14][17]. In [14], target localization is considered in a multistatic ultra wideband radar. The problem is formulated as estimation of target position, which is solved using three methods. Taylor series method is shown to have smaller estimation errors than either least-squares or spherical-interpolation method in a system with one transmitter and four receivers. In [10], two methods are presented to estimate the position of a target in a multistatic passive radar. The spherical-intersection method is shown to be better than the spherical-interpolation method in a system with four transmitters and one receiver. In [6], target localization is investigated in a multistatic passive radar system with one receiver when the receiver position is subject to random errors. An approximated maximum likelihood optimization problem is formulated and solved by a semidefinite relaxation combined with bisection method. In [17], target localization based on both time of arrival and angle of arrival measurements in a multistatic radar system is formulated and a weighted least square method is proposed to estimate the target location. TOA measurements can be used to estimate the position but not the velocity, range rate measurements are needed for the velocity.

In our previous work [7][8], a strategy for collision warning in a three-dimensional (3-D) space was pre-

TABLE I
Target motion parameter observability summary.

Scenario	Sensor configuration	Number of transmitters	Observability
2-D	bistatic	1	marginally observable
2-D	multistatic	2	observable
3-D	bistatic	1	unobservable
3-D	multistatic	2	marginally observable
3-D	multistatic	3	observable

sented, assuming a constant velocity motion of an aircraft of interest (target/intruder), to estimate the position and velocity of the target so as to predict the closest point of approach (CPA). Since an inexpensive system is the goal, only bistatic range and range rate measurements are available. Several configurations listed in Table I are investigated from a parameter observability point of view. In general 3-D scenarios, the target motion parameter is shown to be unobservable in a bistatic configuration (that is: one transmitter and one receiver, not co-located) and a change of course of the receiver (the "observability platform maneuver" that is the saving grace for angle-only target motion analysis (TMA)) merely improves the observability marginally. In a multistatic configuration, one has marginal observability using two transmitters, but good observability with three. In a 2-D scenario which assumes that the target is at the same altitude as the ownship, the target parameter is still only marginally observable in a bistatic configuration. The observability is improved by a small maneuver of the ownship but it is still unappealing. On the other hand, one can have very good observability of the target motion parameter with two transmitters in a 2-D multistatic configuration with the same-altitude assumption, which turns out to be another practically useful configuration in addition to a 3-D multistatic configuration with three transmitters. Simulation results and comparison with the CRLB show that the ML estimate of the target parameter can be considered as statistically efficient in both useful configurations.

The collision warning is formulated as a hypothesis testing problem using a generalized likelihood function. Monte Carlo simulation shows the likelihood-based collision warning algorithm using three transmitters has no missed detection of a collision and has no false alarms when the intruder and ownship altitude separation is beyond 100 m. The likelihood-based collision warning algorithm using two transmitters with the same-altitude assumption has no missed detection of a collision, either. It is, however, prone to false alarms when the CPA angle is near 180°.

This paper extends the previous work [7][8] by (i) taking the physical dimensions of aircraft into consideration in the likelihood-based collision warning algorithm; (ii) investigating the statistical efficiency of the closest point of approach (CPA) time estimate in the likelihood-based collision warning algorithm; (iii) adding a Bayesian approach for collision warning. Since air collision is deadly, no missed detections can be tolerated. It is also necessary to account for the physical dimensions of aircraft by adding a safety margin to compensate for the errors arising in the point modeling of aircraft. Simulation results show that the likelihood-based collision warning algorithm with a safety margin of 100 m has no missed detections of collision but becomes more conservative with false alarms occurring in more situations.

The likelihood based collision warning algorithm makes decisions by using an estimated CPA time, and Monte Carlo simulations have shown that the CPA time estimate can be considered as unbiased and statistically efficient for the simulated scenarios. The Bayesian approach formulates the CPA distance as a random variable and estimates its probability density function (pdf) as a fitted Rician distribution. Then it defines the collision event by considering the physical dimensions of the aircraft and calculates the probability of collision, based on which a warning decision can be made. The performance of the Bayesian collision warning algorithm is consistent with that of a likelihood-based algorithm.

The remaining sections of this paper are organized as follows. Section 2 describes and formulates the general 3-D problem and considers a special 2-D problem. Section 3 analyzes several possible configurations for collision warning including both 3-D and 2-D scenarios and shows that two of them seem to be practically useful. Section 4 presents the ML estimator based on which two different collision warning algorithms are described in Section 5. Section 6 investigates the efficiency of the ML estimator of the target motion parameter and the efficiency of the CPA time estimate used in the likelihood-based collision warning algorithm, and also shows the performances of both collision warning algorithms and Section 7 draws conclusions.

2. PROBLEM FORMULATION

Assume a target of interest (intruder) is moving in 3-D with a constant velocity. The 3-D target position in Cartesian coordinates at time k is therefore

$$\boldsymbol{\xi}(\mathbf{x},k) = \mathbf{x}_0 + kT\dot{\mathbf{x}}_0 \quad k = 0,1,\ldots \tag{1}$$

where

$$\mathbf{x} = [\mathbf{x}_0', \dot{\mathbf{x}}_0']' = [x, y, z, \dot{x}, \dot{y}, \dot{z}]' \tag{2}$$

is the unknown target motion parameter which is a vector of dimension $n_{\mathbf{x}} = 6$ consisting of the target's position $\mathbf{x}_0$ and velocity $\dot{\mathbf{x}}_0$ in Cartesian coordinates at time $k = 0$ (or without loss of generality at any chosen reference time); and T is the sampling period. There are N_{Tx} ($N_{\mathrm{Tx}} \geq 1$) transmitters at known locations $\mathbf{u}_i = [x_{u_i}, y_{u_i}, z_{u_i}]'$, $i = 1,\ldots,N_{\mathrm{Tx}}$. At time k ($k > 0$), a moving receiver (the ownship) with known position $\mathbf{s}(k)$ and velocity $\dot{\mathbf{s}}(k)$ can obtain measurements consisting of the

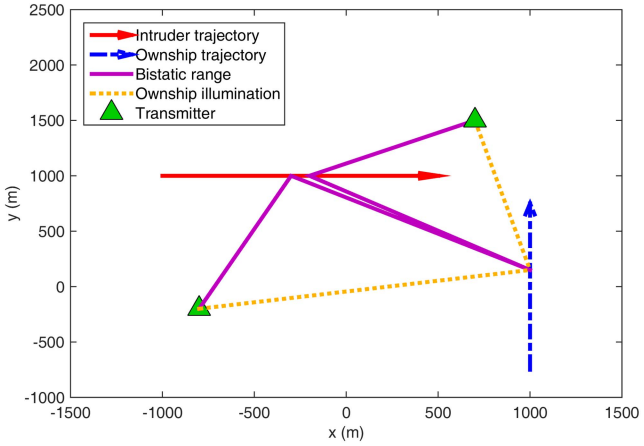

Fig. 1. A multistatic configuration in the X-Y plane. The time differences of arrival (actual measurements) between the direct path (ownship illumination) and the indirect path (bistatic range) multiplied by the speed of light is added to the direct path distance to yield an equivalent bistatic range measurement.

bistatic range [4] illustrated in Figure 1 and the bistatic range rate from the ith transmitter located at $\mathbf{u}_i$ given by

$$\mathbf{z}_i(k) = \mathbf{h}_i(\mathbf{x},k) + \mathbf{w}_i(k) \quad i = 1,\ldots,N_{\text{Tx}} \tag{3}$$

where

$$\mathbf{h}_i(\mathbf{x},k) = \begin{bmatrix} r_i(k) \\ \dot{r}_i(k) \end{bmatrix} = \begin{bmatrix} \|\boldsymbol{\xi}(\mathbf{x},k) - \mathbf{s}(k)\| + \|\boldsymbol{\xi}(\mathbf{x},k) - \mathbf{u}_i\| \\ \dfrac{[\boldsymbol{\xi}(\mathbf{x},k) - \mathbf{s}(k)]'[\dot{\mathbf{x}}_0 - \dot{\mathbf{s}}(k)]}{\|\boldsymbol{\xi}(\mathbf{x},k) - \mathbf{s}(k)\|} + \dfrac{[\boldsymbol{\xi}(\mathbf{x},k) - \mathbf{u}_i]'\dot{\mathbf{x}}_0}{\|\boldsymbol{\xi}(\mathbf{x},k) - \mathbf{u}_i\|} \end{bmatrix} \tag{4}$$

and $\mathbf{w}_i(k)$ are the measurement noises, assumed to be independent and identically distributed zero-mean white Gaussian sequences with known covariance matrix

$$R_i = \begin{bmatrix} \sigma_r^2 & 0 \\ 0 & \sigma_{\dot{r}}^2 \end{bmatrix} \tag{5}$$

The measurement function comprising all the measurements at time k is

$$\mathbf{z}(k) = \mathbf{h}(\mathbf{x},k) + \mathbf{w}(k) \quad k = 1,\ldots \tag{6}$$

where

$$\mathbf{z}(k) = [\mathbf{z}_1(k)' \ldots \mathbf{z}_{N_{\text{Tx}}}(k)']' \tag{7}$$

$$\mathbf{h}(\mathbf{x},k) = [\mathbf{h}_1(\mathbf{x},k)' \ldots \mathbf{h}_{N_{\text{Tx}}}(\mathbf{x},k)']' \tag{8}$$

$$\mathbf{w}(k) = [\mathbf{w}_1(k)' \ldots \mathbf{w}_{N_{\text{Tx}}}(k)']' \tag{9}$$

and

$$R(k) = E[\mathbf{w}(k)\mathbf{w}(k)'] = \begin{bmatrix} R_1 & \mathbf{0} & \cdots & \mathbf{0} \\ \mathbf{0} & R_2 & \cdots & \mathbf{0} \\ \vdots & \vdots & \ddots & \vdots \\ \mathbf{0} & \mathbf{0} & \cdots & R_{N_{\text{Tx}}} \end{bmatrix} \tag{10}$$

Since both intruder and ownship are moving, it is important to avoid any collision between them. The goal is thus to estimate the target parameter $\mathbf{x}$ based on N frames of measurements, and to deliver a warning long enough and confidently enough before a possible collision occurs so as to predict the CPA and, presumably, to do something about it if needed.

2.1. Parameter Observability

We need to check the observability of the target motion parameter (2) to see whether there is sufficient information in the data. Observability requires the invertibility of the Fisher information matrix (FIM), which is given by [3]

$$J = E\{[\nabla_{\mathbf{x}} \ln \Lambda(\mathbf{x};\mathbf{Z})][\nabla_{\mathbf{x}} \ln \Lambda(\mathbf{x};\mathbf{Z})]'\}|_{\mathbf{x}=\mathbf{x}_t} \tag{11}$$

where $\Lambda(\mathbf{x};\mathbf{Z})$ is the likelihood function of the parameter based on the measurement set

$$\mathbf{Z} = \mathbf{z}(k)_{k=1}^{N} \tag{12}$$

and $\mathbf{x}_t$ is the true value of the target motion parameter. In a simulated scenario, $\mathbf{x}_t$ is known. However, in a real scenario where $\mathbf{x}_t$ is unknown and needs to be estimated, the FIM is evaluated at the estimate.

Since the measurement noises are assumed to be white, we have

$$\Lambda(\mathbf{x};\mathbf{Z}) = \prod_{k=1}^{N} p(\mathbf{z}(k) \mid \mathbf{x}) \tag{13}$$

where

$$p(\mathbf{z}(k) \mid \mathbf{x}) = |2\pi R(k)|^{-1/2} \cdot \exp(-\tfrac{1}{2}[\mathbf{z}(k) - \mathbf{h}(\mathbf{x},k)]'R(k)^{-1}[\mathbf{z}(k) - \mathbf{h}(\mathbf{x},k)]) \tag{14}$$

The gradient of the log-likelihood function is

$$\nabla_{\mathbf{x}} \ln \Lambda(\mathbf{x};\mathbf{Z}) = -\sum_{k=1}^{N} [\nabla_{\mathbf{x}} \mathbf{h}(\mathbf{x},k)']R(k)^{-1}[\mathbf{z}(k) - \mathbf{h}(\mathbf{x},k)] \tag{15}$$

Substituting (15) into (11) yields

$$J = \sum_{k=1}^{N} [\nabla_{\mathbf{x}} \mathbf{h}(\mathbf{x},k)']R(k)^{-1}[\nabla_{\mathbf{x}} \mathbf{h}(\mathbf{x},k)']'|_{\mathbf{x}=\mathbf{x}_t} = \sum_{k=1}^{N} \sum_{i=1}^{N_{\text{Tx}}} [\nabla_{\mathbf{x}} \mathbf{h}_i(\mathbf{x},k)']R_i^{-1}[\nabla_{\mathbf{x}} \mathbf{h}_i(\mathbf{x},k)']'|_{\mathbf{x}=\mathbf{x}_t} \tag{16}$$

If J is not invertible, then the target motion parameter is unobservable. Otherwise, the size of confidence region for the true target position [3] can be used to distinguish between marginal observability and good observability. In this paper, marginal and good observability are distinguished from each other by the length of the longest semiaxis of 99.9999% probability region. In the application of air collision warning, one could say that the observability is good if the longest semiaxis is, say, less than 100 meters and that the observability is marginal if the longest semiaxis is, say, more than

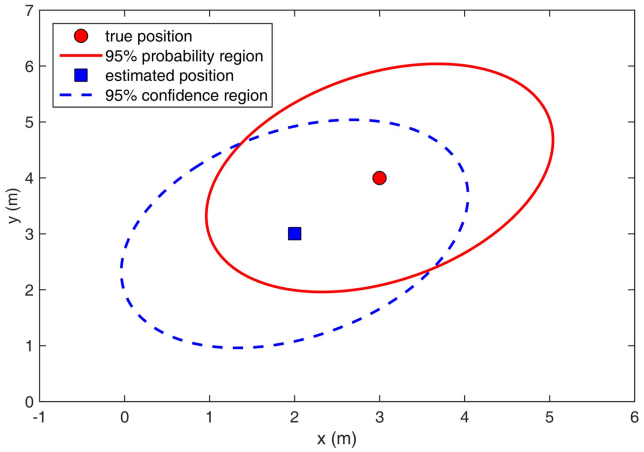

Fig. 2. Confidence region and probability region in the X-Y plane. If an estimate is inside 95% probability region around the truth, then the truth must be inside 95% confidence region around this estimate.

100 meters. Mathematically, the length of the longest semiaxis is proportional to the square root of largest eigenvalue of the covariance matrix in (20).

2.2. Confidence Region in the General Case

Suppose one has an unbiased and statistically efficient estimate $\hat{\mathbf{x}}$, that is

$$E[\hat{\mathbf{x}}] = \mathbf{x}_{\mathrm{t}} \tag{17}$$

$$P \triangleq E[[\hat{\mathbf{x}} - \mathbf{x}_{\mathrm{t}}][\hat{\mathbf{x}} - \mathbf{x}_{\mathrm{t}}]'] = J^{-1} \tag{18}$$

where J^{-1} is the Cramer Rao lower bound (CRLB). The 3-D target position estimate at an arbitrary time t is

$$\hat{\mathbf{x}}_{\mathrm{p}}(t) = \begin{bmatrix} 1 & 0 & 0 & t & 0 & 0 \\ 0 & 1 & 0 & 0 & t & 0 \\ 0 & 0 & 1 & 0 & 0 & t \end{bmatrix} \hat{\mathbf{x}} \triangleq \Phi_{\mathrm{p}}(t)\hat{\mathbf{x}} \tag{19}$$

and the corresponding covariance is

$$P_{\mathrm{p}}(t) = \Phi_{\mathrm{p}}(t) P \Phi_{\mathrm{p}}(t)' \tag{20}$$

If one further assumes $\hat{\mathbf{x}}$ is Gaussian, that is,

$$\hat{\mathbf{x}} \sim \mathcal{N}(\mathbf{x}_{\mathrm{t}}, P) \tag{21}$$

then, because of linear transformation in (19)

$$\hat{\mathbf{x}}_{\mathrm{p}}(t) \sim \mathcal{N}(\mathbf{x}_{\mathrm{p}}(t), P_{\mathrm{p}}(t)) \tag{22}$$

The normalized estimation error squared (NEES) for the target position $\mathbf{x}_{\mathrm{p}}(t)$ at t, defined as

$$\epsilon_{\mathrm{p}}(t) = [\mathbf{x}_{\mathrm{p}}(t) - \hat{\mathbf{x}}_{\mathrm{p}}(t)]' P_{\mathrm{p}}^{-1}(t) [\mathbf{x}_{\mathrm{p}}(t) - \hat{\mathbf{x}}_{\mathrm{p}}(t)] \tag{23}$$

is chi-square distributed with $n_{\mathbf{x}}/2$ degrees of freedom, that is,

$$\epsilon_{\mathrm{p}}(t) \sim \chi^2_{n_x/2} \tag{24}$$

Let g be such that

$$P\{\epsilon_{\mathrm{p}}(t) \leq g^2\} = 1 - Q \tag{25}$$

where Q is a small tail probability. Given the predicted target position $\hat{\mathbf{x}}_{\mathrm{p}}(t)$, the $100(1-Q)\%$ confidence region [2] for the true position $\mathbf{x}_{\mathrm{p}}(t)$ is defined to be within the ellipsoid given by

$$[\mathbf{x}_{\mathrm{p}}(t) - \hat{\mathbf{x}}_{\mathrm{p}}(t)]' P_{\mathrm{p}}^{-1}(t) [\mathbf{x}_{\mathrm{p}}(t) - \hat{\mathbf{x}}_{\mathrm{p}}(t)] = g^2 \tag{26}$$

Alternatively, given the true position $\mathbf{x}_{\mathrm{p}}(t)$, (26) is also defined to be the $100(1-Q)\%$ probability region for the predicted target position $\hat{\mathbf{x}}_{\mathrm{p}}(t)$. These two regions as shown in Figure 2 have identical geometrical sizes since they can be represented by the same equation as in (26). If either region is large, one has marginal observability of the target position; if any one of the regions is small, one has good observability of the target position.

2.3. Confidence Region When Intruder and Ownship at Same Altitude

If the intruder's altitude z is assumed to be known and is equal to that of the ownship, then the 2-D X-Y plane at the altitude z is of interest and everything related to the target can be considered restricted to this 2-D space. Specifically, the target parameter to be estimated becomes

$$\mathbf{x}^{\mathrm{2D}} = [x, y, \dot{x}, \dot{y}]' \tag{27}$$

Correspondingly, the 2-D target position at an arbitrary time t is

$$\mathbf{x}_{\mathrm{p}}^{\mathrm{2D}}(t) = \begin{bmatrix} 1 & 0 & t & 0 \\ 0 & 1 & 0 & t \end{bmatrix} \mathbf{x}^{\mathrm{2D}} \tag{28}$$

The confidence region for the true target position around its estimate is now an ellipse given by (26).

3. SCENARIOS AND OBSERVABILITY ANALYSIS

From (26), the size of the confidence region for the true target position around the predicted position is the same as that of the probability region for the predicted target position around the true position. Since it is more convenient for an observability analysis to obtain the probability region for the predicted target position with the true target motion parameter assumed available than to estimate the true target parameter and obtain the confidence region for it, in this section several scenarios are simulated with the knowledge of the true target motion parameter and the probability region of the estimate in each scenario is obtained without performing any estimation.

A radar system, which consists of three transmitters on the ground and one receiver mounted on an unmanned aircraft system (UAS)—the ownship—is used to warn of a possible collision between the UAS (ownship) and an intruder aircraft. The transmitters are located at (0 m, 1000 m, 0 m), (0 m, −1000 m, 0 m) and (1000 m, 0 m, 0 m) in Cartesian coordinates, and

TABLE II
Scenario specifications. The last column reflects the results from Section 3.

Scenario	Transmitters used	UAS motion	Target altitude	Collision	Semiaxis lengths of 99.9999% probability region (m)
1	Tx1	CV	Unknown	Yes	3×10^9, 2020, 62
2	Tx1	two-segment CV	Unknown	Yes	6468, 1660, 109
3	Tx1 and Tx2	CV	Unknown	Yes	1542, 50, 41
4	Tx1 and Tx2	two-segment CV	Unknown	Yes	1402, 51, 41
5	Tx1,Tx2 and Tx3	CV	Unknown	Yes	50, 42, 11
6	Tx1,Tx2 and Tx3	CV	Unknown	No	48, 43, 12
7	Tx1	CV	Known	Yes	2600, 81
8	Tx1	two-segment CV	Known	Yes	301, 25
9	Tx1 and Tx2	CV	Known	Yes	40, 8

are denoted by Tx1, Tx2 and Tx3, respectively. The UAS is moving at an altitude of 1500 m.

Eight collision scenarios and one non-collision scenario listed in the Table II, differing in the number of transmitters, the motion of the UAS and the dimensionality of target parameter are studied here. Scenarios with the "known target altitude" assumption are referred to as 2-D scenarios. The rest are 3-D scenarios. Two motions of UAS are considered. In a constant velocity (CV) motion, the UAS starts moving from the point (−4500 m, 0 m, 1500 m) at time $t = 0$ s with a constant velocity $\dot{\mathbf{s}}_0 = [50\text{m/s}, 0\text{ m/s}, 0\text{ m/s}]'$. In a two-segment CV motion, the UAS starts with a constant velocity [43 m/s, − 25 m/s, 0 m/s]′ from the point (−4306 m, 752 m, 1500 m) at time $t = 0$ s for 27 s and then executes a 5°/s coordinated turn for 6 s before changing to another velocity [50 m/s, 0 m/s, 0 m/s]′ when it arrives at the location (−2850 m, 0 m, 1500 m). In all the collision scenarios, the intruder aircraft starts from the position (4500 m, 0 m, 1500 m) at time $t = 0$ s with a constant velocity $\dot{\mathbf{x}}_0 = [-50\text{ m/s}, 0\text{ m/s}, 0\text{ m/s}]'$ and will collide with the UAS at time $t = 90$ s. In the non-collision scenario, the altitude of the intruder aircraft is assumed to be 1600 m, which is 100 m higher than in the collision scenarios, and the CPA occurs at time $t = 90$ s. Bistatic range and range rate measurements are made from the ownship every 1 s over a period of 60 s, which is 30 s before the CPA time. The noise standard deviations for the range and range rate measurements are assumed to be 8.66 m and 1 m/s, respectively, at all times.

Figures 3 and 4 visualize all the 3-D scenarios and plots the 99.9999% probability region, the lengths of the semiaxes of which are also shown in Table II, around the collision point or the target CPA in each scenario.

In Scenario 1, the FIM is nearly singular with a condition number[1] of 18.8. The large probability region (which implies a large confidence region) indicates the target parameter is practically unobservable and even an efficient estimator is useless in such a situation.

[1]The condition number is $\log_{10}(\lambda_{\max}/\lambda_{\min})$, where $\lambda_{\max}$ and $\lambda_{\min}$ are the largest and smallest eigenvalues of the FIM.

In Scenario 2, the FIM is not ill-conditioned. The ellipsoid is much smaller than in the first scenario, which indicates the change of course in the ownship trajectory improves the observability. However, the size of the probability (or confidence) region is still quite large so that even an efficient estimator remains practically useless.

Compared with the 3-D bistatic configuration (Scenarios 1 and 2), adding a second transmitter in Scenarios 3 and 4 reduces the target localization uncertainty, although the size of the probability region is still too large to be useful. Comparison between Figures 3(c) and 3(d) indicates that the further reduction of the localization uncertainty resulting from the change of course in the ownship trajectory in the multistatic configuration is not as significant as in the bistatic.

As shown in Figures 4(a) and 4(b), the addition of a third transmitter into the multistatic configuration has significantly improved observability, which makes the localization practically useful. Therefore, one needs three transmitters in a 3-D multistatic configuration to build up an efficient estimator based on which a useful collision warning algorithm can be designed.

Figure 5 visualizes all the 2-D scenarios and plots the 99.9999% probability region around the collision point in each scenario. Compared with 3-D scenarios, the knowledge of target altitude in a 2-D scenario results in a significant reduction in the uncertainty. In Scenario 7, the size of the probability region is still too large to be useful. In Scenario 8, the probability region could be useful, however, it is due to the change of course of the ownship and this maneuver action itself could lead a safety situation to a dangerous collision. In Scenario 9, adding a second transmitter reduces the target localization uncertainty significantly. The size of this region is practically useful. Therefore, with the knowledge of the target altitude one needs two transmitters in a multistatic configuration to build up an efficient estimator based on which a useful collision warning algorithm can be designed.

In the sequel, collision warning is only considered in those two practically useful configurations—3 transmitters in general 3-D scenarios and 2 transmitters with

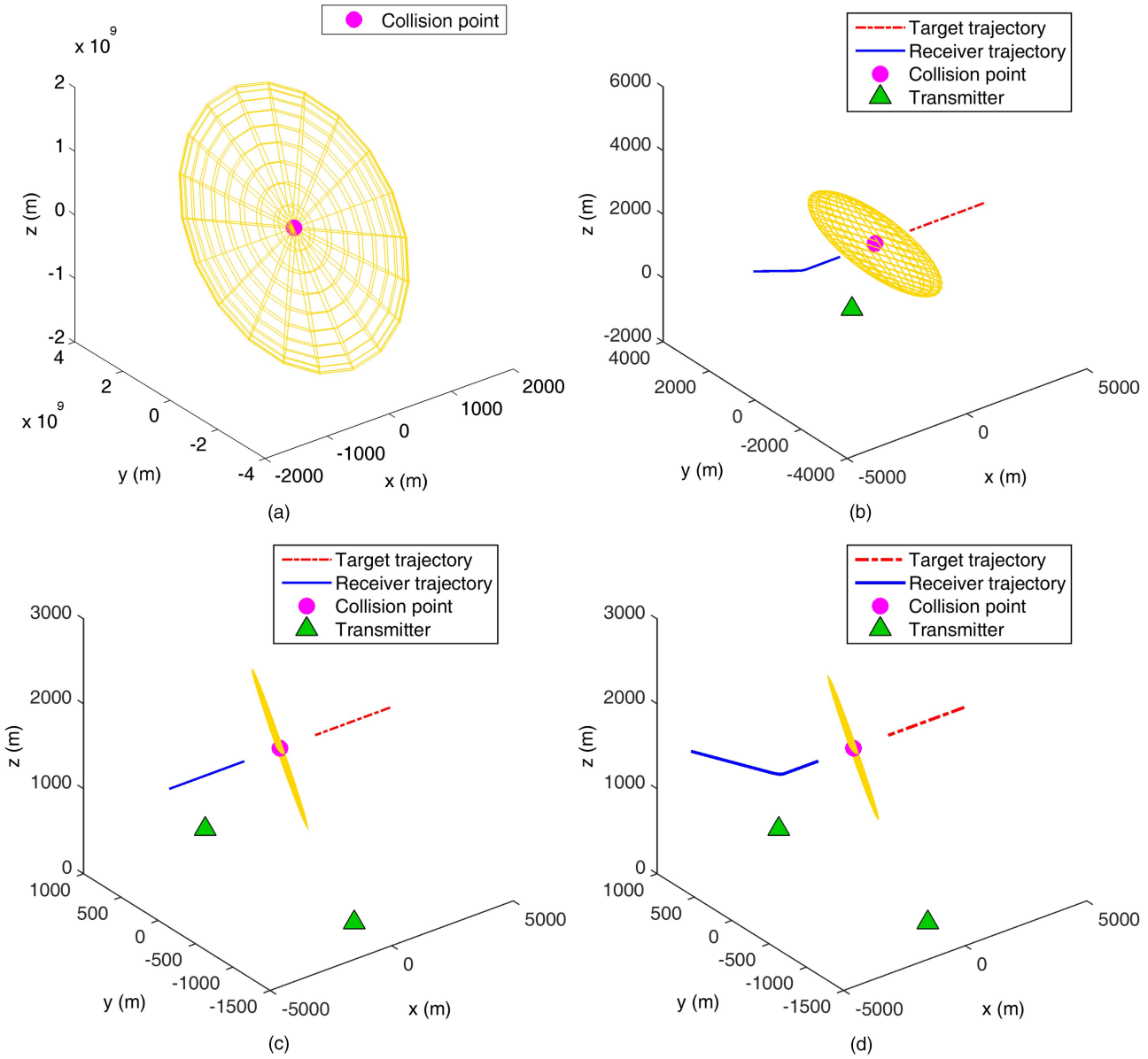

Fig. 3. 99.9999% (ellipsoidal) probability region around the collision point in Scenarios 1 to 4. The target motion parameter is practically unobservable in Scenario 1. The target motion parameter is marginally observable in Scenarios 2, 3 and 4. (a) Scenario 1. (b) Scenario 2. (c) Scenario 3. (d) Scenario 4.

known target altitude in 2-D scenarios, corresponding to Scenarios 5, 6 and 9.

4. THE MAXIMUM LIKELIHOOD ESTIMATOR

The ML estimate of the target motion parameter $\mathbf{x}$ in (2) is

$$\hat{\mathbf{x}}_{\mathrm{ML}} = \arg\max_{\mathbf{x}} \Lambda(\mathbf{x};\mathbf{Z}) \tag{29}$$

where $\Lambda(\mathbf{x};\mathbf{Z})$ is given in (13). The ILS technique [2] was used to find the ML estimate in this case. If we set (15) to zero, we will notice that there is no closed-form solution. Using a first order series expansion about an estimate $\hat{\mathbf{x}}^j$ at the end of the jth iteration leads to an iterative scheme and the $(j+1)$th estimate is

$$\hat{\mathbf{x}}^{j+1} = \hat{\mathbf{x}}^j + [(H^j)'R^{-1}H^j]^{-1}(H^j)'R^{-1}[\mathbf{z} - \mathbf{h}(\hat{\mathbf{x}}^j)] \tag{30}$$

where

$$\mathbf{z} = [\mathbf{z}(1)', \mathbf{z}(2)', \ldots, \mathbf{z}(N)']' \tag{31}$$

$$\mathbf{h}(\hat{\mathbf{x}}^j) = [\mathbf{h}(\hat{\mathbf{x}}^j, 1), \mathbf{h}(\hat{\mathbf{x}}^j, 2), \ldots, \mathbf{h}(\hat{\mathbf{x}}^j, N)]' \tag{32}$$

$$R = \begin{bmatrix} R(1) & \mathbf{0} & \cdots & \mathbf{0} \\ \mathbf{0} & R(2) & \cdots & \mathbf{0} \\ \vdots & \vdots & \ddots & \vdots \\ \mathbf{0} & \mathbf{0} & \cdots & R(N) \end{bmatrix} \tag{33}$$

and

$$H^j = \begin{bmatrix} [\nabla_{\mathbf{x}} \mathbf{h}(\mathbf{x}, 1)']'|_{\mathbf{x}=\hat{\mathbf{x}}^j} \\ [\nabla_{\mathbf{x}} \mathbf{h}(\mathbf{x}, 2)']'|_{\mathbf{x}=\hat{\mathbf{x}}^j} \\ \vdots \\ [\nabla_{\mathbf{x}} \mathbf{h}(\mathbf{x}, N)']'|_{\mathbf{x}=\hat{\mathbf{x}}^j} \end{bmatrix} \tag{34}$$

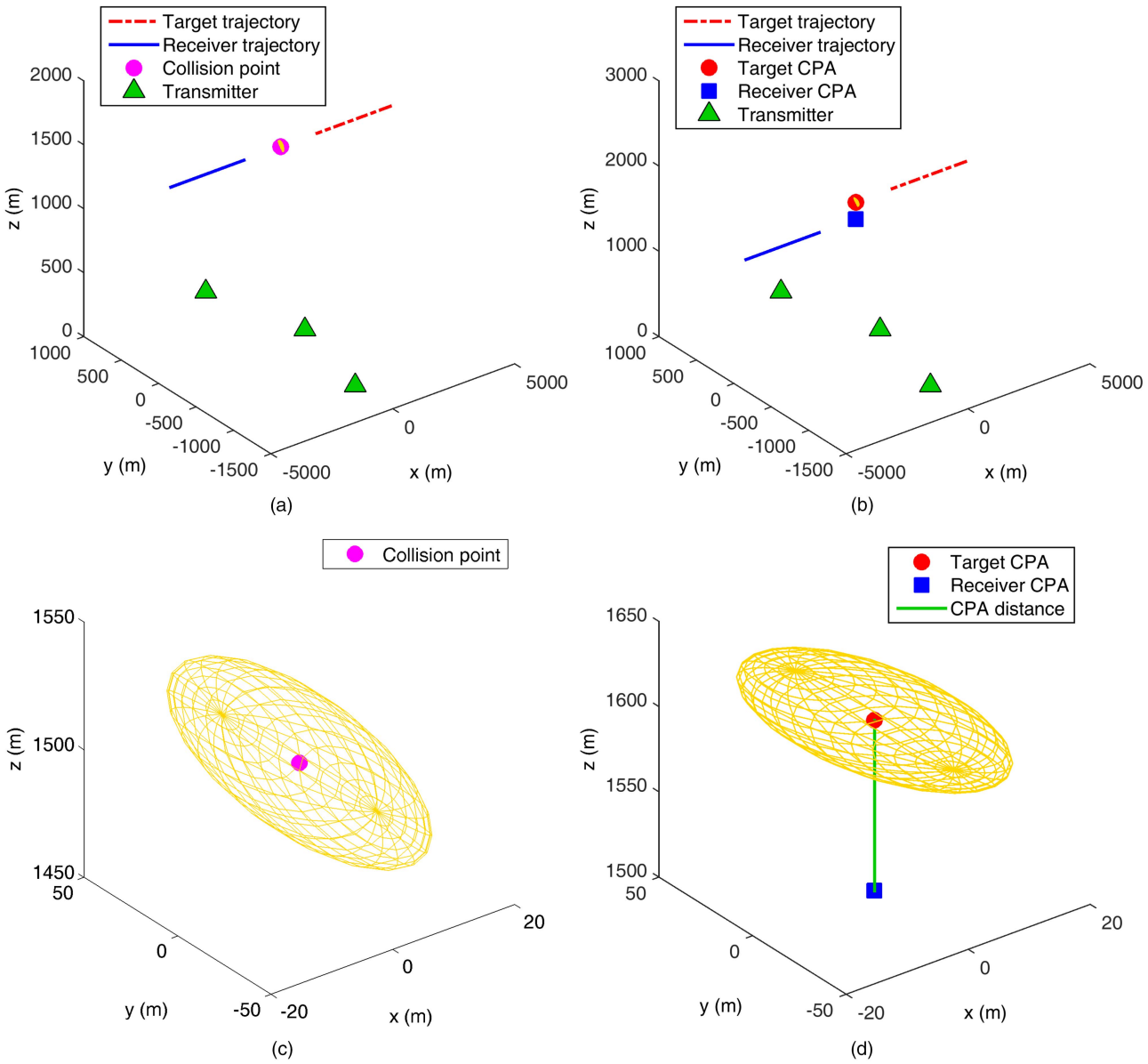

Fig. 4. 99.9999% (ellipsoidal) probability region around the collision point or the target CPA in Scenarios 5 and 6. The target motion parameter observability is good in both scenarios. (a) Scenario 5. (b) Scenario 6. (c) Scenario 5 magnified. (d) Scenario 6 magnified.

An initial estimate can be obtained by solving (3) with the noise set to zero based on the measurements for two transmitters at two different time instants.

The ML estimate of the target parameter $\mathbf{x}_{2D}$ in (27) in a 2-D scenario can be found using the ILS technique in the same manner.

This paper assumes that a fixed number N of frames of measurements are processed together using a batch approach. Therefore, there is no need to use a recursive algorithm for sequential update. One can sequentially process the measurements using a recursive estimator as more and more measurements are received. For example, the probability region considered in this paper will become smaller and smaller as more and more measurements are used in the target parameter estimation. The decision on collision warning can be made earlier before N frames of measurements become available. However, since the problem is highly nonlinear, a recursive estimator would be by necessity suboptimal, either due to linearization or using a particle filter. We will consider this in the future: This is a topic for future investigation.

5. COLLISION WARNING APPROACHES

5.1. Collision Warning via Hypothesis Testing Based on a Generalized Likelihood Function

The collision event at time t (t to be determined) is defined by equating the true target position $\mathbf{x}_p(t)$ to the ownship position, namely,

$$\{\text{Collision at } t\} \triangleq \{\mathbf{x}_p(t) = \mathbf{s}(t)\} \tag{35}$$

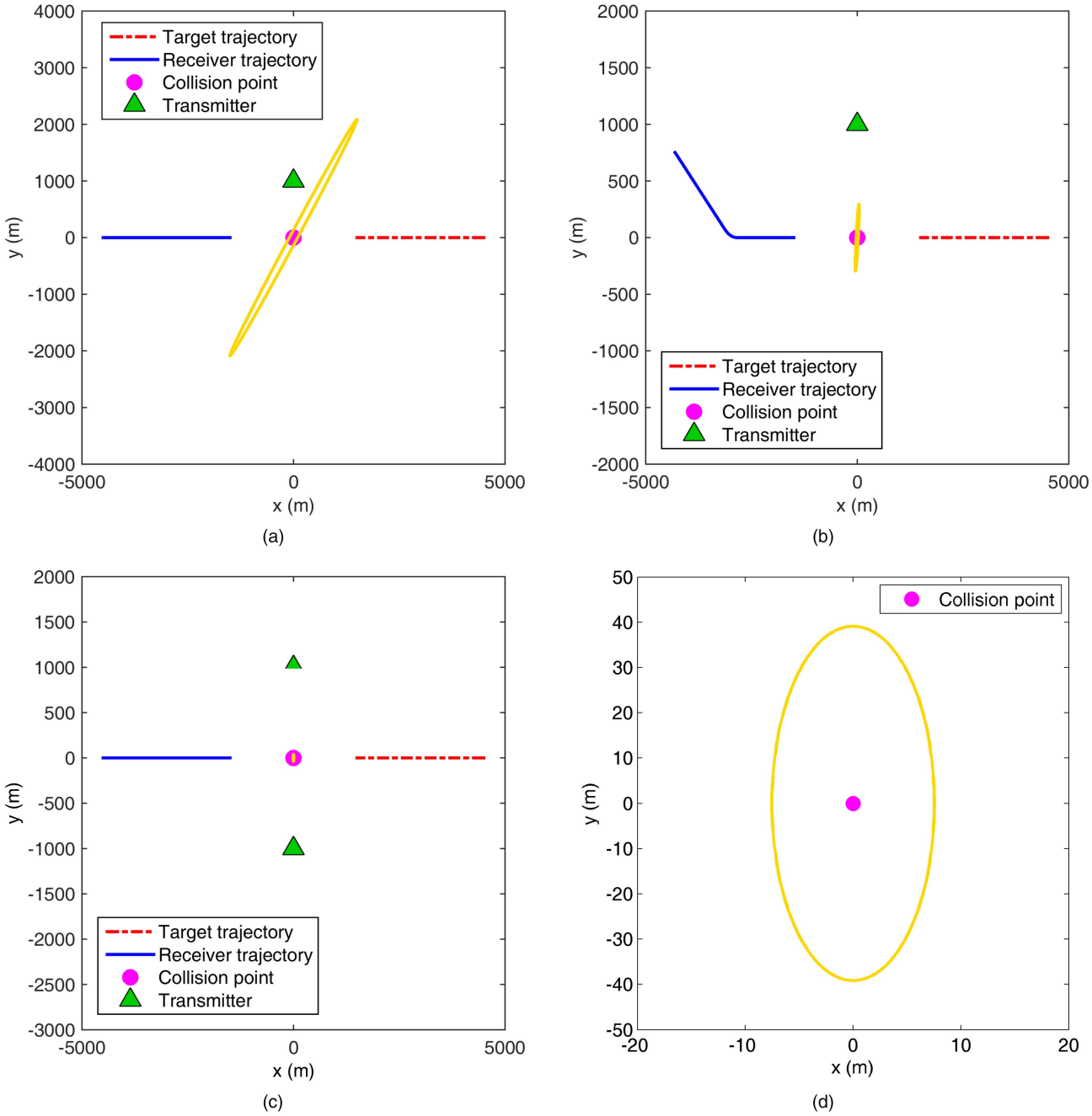

Fig. 5. 99.9999% (elliptic) probability region around the collision point in 2-D scenarios. The target motion parameter is marginally observable in Scenarios 7 and 8. The target motion parameter observability is good in Scenario 9. (a) Scenario 7. (b) Scenario 8. (c) Scenario 9. (d) Scenario 9 magnified.

Following [2], the likelihood function of collision is the pdf of the predicted target position to time t (the "observation" based on which the collision warning can be made) conditioned on (35)

$$\begin{aligned}\Lambda[\mathbf{x}_{\mathrm{p}}(t)=\mathbf{s}(t);\hat{\mathbf{x}}_{\mathrm{p}}(t)] &= p[\hat{\mathbf{x}}_{\mathrm{p}}(t)\mid \mathbf{x}_{\mathrm{p}}(t)=\mathbf{s}(t)]\\ &= \mathcal{N}[\hat{\mathbf{x}}_{\mathrm{p}}(t);\mathbf{s}(t),P_{\mathrm{p}}(t)] = |2\pi P_{\mathrm{p}}(t)|^{-1/2}\\ &\quad\cdot\exp(-\tfrac{1}{2}[\hat{\mathbf{x}}_{\mathrm{p}}(t)-\mathbf{s}(t)]' P_{\mathrm{p}}^{-1}(t)[\hat{\mathbf{x}}_{\mathrm{p}}(t)-\mathbf{s}(t)])\end{aligned} \tag{36}$$

where $\hat{\mathbf{x}}_{\mathrm{p}}(t)$ is given by (19). The use of the covariance $P_{\mathrm{p}}(t)$ in (36) is justified based on the discussion presented in Section 6, which validates the efficiency of (29).

Since the time t in (36) is not known, we estimate the CPA time as

$$\hat{t}_{\mathrm{CPA}} = \arg\max_{t} \Lambda[\mathbf{x}_{\mathrm{p}}(t)=\mathbf{s}(t);\hat{\mathbf{x}}_{\mathrm{p}}(t)] \tag{37}$$

The CPA time estimate is found by using the Quasi-Newton method with a cubic line search procedure. The search starts with an initial value, which can be obtained using (58) by considering the estimated target parameter

as deterministic. For the purpose of simulations, the MATLAB function "fminunc" is used.

The collision warning can be formulated as a hypothesis testing problem as follows. The two hypotheses are, based on (37)

$$H_0 : \mathbf{x}_{\mathrm{p}}(\hat{t}_{\mathrm{CPA}}) = \mathbf{s}(\hat{t}_{\mathrm{CPA}}) \tag{38}$$

$$H_1 : \mathbf{x}_{\mathrm{p}}(\hat{t}_{\mathrm{CPA}}) \neq \mathbf{s}(\hat{t}_{\mathrm{CPA}}) \tag{39}$$

The (generalized[2]) likelihood function for H_0 is

$$\begin{aligned}\Lambda[H_0; \hat{\mathbf{x}}_{\mathrm{p}}(\hat{t}_{\mathrm{CPA}})] &= \mathcal{N}[\hat{\mathbf{x}}_{\mathrm{p}}(\hat{t}_{\mathrm{CPA}}); \mathbf{s}(\hat{t}_{\mathrm{CPA}}), P_{\mathrm{p}}(\hat{t}_{\mathrm{CPA}})] \\ &= \mathcal{N}[\mathbf{s}(\hat{t}_{\mathrm{CPA}}); \hat{\mathbf{x}}_{\mathrm{p}}(\hat{t}_{\mathrm{CPA}}), P_{\mathrm{p}}(\hat{t}_{\mathrm{CPA}})]\end{aligned} \tag{40}$$

For a given level of significance, say 0.0001% (assuming this is the desired confidence to avoid collision, $Q = 10^{-6}$ in (25)), there are two equivalent procedures to determine whether H_0 should be rejected.

Procedure 1: one computes

$$\epsilon = [\hat{\mathbf{x}}_{\mathrm{p}}(\hat{t}_{\mathrm{CPA}}) - \mathbf{s}(\hat{t}_{\mathrm{CPA}})]' P_{\mathrm{p}}^{-1}(\hat{t}_{\mathrm{CPA}})[\hat{\mathbf{x}}_{\mathrm{p}}(\hat{t}_{\mathrm{CPA}}) - \mathbf{s}(\hat{t}_{\mathrm{CPA}})] \tag{41}$$

and

$$\epsilon_{\mathrm{th}} = F_{\chi^2}^{-1}(1 - Q, n_{\mathrm{dof}}) \tag{42}$$

where $F_{\chi^2}^{-1}$ is the inverse of the cumulative distribution function (cdf) of a chi-square random variable with n_{dof} degrees of freedom. If

$$\epsilon > \epsilon_{\mathrm{th}} \tag{43}$$

then $\mathbf{s}(\hat{t}_{\mathrm{CPA}})$ is outside the 99.9999% confidence region centered at $\hat{\mathbf{x}}_{\mathrm{p}}(\hat{t}_{\mathrm{CPA}})$, then one can say that collision is unlikely ($< 0.0001\%$). Otherwise a collision warning is issued.

Procedure 2: one computes

$$\epsilon = [\hat{\mathbf{x}}_{\mathrm{p}}(\hat{t}_{\mathrm{CPA}}) - \mathbf{s}(\hat{t}_{\mathrm{CPA}})]' P_{\mathrm{p}}^{-1}(\hat{t}_{\mathrm{CPA}})[\hat{\mathbf{x}}_{\mathrm{p}}(\hat{t}_{\mathrm{CPA}}) - \mathbf{s}(\hat{t}_{\mathrm{CPA}})] \tag{44}$$

and estimates the probability of collision as

$$\mathrm{P}_c = 1 - F_{\chi^2}(\epsilon, n_{\mathrm{dof}}) \tag{45}$$

where F_{χ^2} is the cdf of a chi-square random variable with n_{dof} degrees of freedom. If

$$\mathrm{P}_c > 0.0001\% \tag{46}$$

then a collision warning is alerted.

These two procedures are equivalent because of the invertibility of the cdf of the chi-square distribution.

So far, both the target and the ownship have been modeled as points of zero size. If one takes the physical dimensions of both the target and the ownship into consideration, a safety margin Δd (which would, typically, be more than the sum of the target and ownship sizes) is needed in the decision making. In this case, the definition of the collision event in (35) will be modified to be

$$\{\text{Collision at } t\} \stackrel{\Delta}{=} \{\|\mathbf{x}_{\mathrm{p}}(t) - \mathbf{s}(t)\| \leq \Delta d\} \tag{47}$$

and the hypotheses in (38) and (39) will be modified as

$$H_0 : \|\mathbf{x}_{\mathrm{p}}(t) - \mathbf{s}(t)\| \leq \Delta d \tag{48}$$

$$H_1 : \|\mathbf{x}_{\mathrm{p}}(t) - \mathbf{s}(t)\| > \Delta d \tag{49}$$

Therefore, H_0 in (48) is rejected at a level of 0.0001% if $\mathbf{s}(\hat{t}_{\mathrm{CPA}})$ is outside the 99.9999% confidence region centered at $\hat{\mathbf{x}}_{\mathrm{p}}(\hat{t}_{\mathrm{CPA}})$ and

$$\Delta d < \min_{\mathbf{x}} \|\mathbf{s}(\hat{t}_{\mathrm{CPA}}) - \mathbf{x}\| \tag{50}$$

subject to

$$\begin{aligned}&[\hat{\mathbf{x}}_{\mathrm{p}}(\hat{t}_{\mathrm{CPA}}) - \mathbf{x}]' P_{\mathrm{p}}^{-1}(\hat{t}_{\mathrm{CPA}})[\hat{\mathbf{x}}_{\mathrm{p}}(\hat{t}_{\mathrm{CPA}}) - \mathbf{x}] \\ &\quad = F_{\chi^2}^{-1}(0.999999, n_{\mathrm{dof}})\end{aligned} \tag{51}$$

that is, the minimum distance between $\mathbf{s}(\hat{t}_{\mathrm{CPA}})$ and any point on the surface of the 99.9999% confidence region is larger than Δd.

Equivalently, in a similar way to (44)–(46), one can also estimate the probability of collision as

$$\mathrm{P}_c = 1 - F_{\chi^2}(\epsilon_{\min}, n_{\mathrm{dof}}) \tag{52}$$

where

$$\epsilon_{\min} = \min_{\mathbf{x}} [\hat{\mathbf{x}}_{\mathrm{p}}(\hat{t}_{\mathrm{CPA}}) - \mathbf{x}]' P_{\mathrm{p}}^{-1}(\hat{t}_{\mathrm{CPA}})[\hat{\mathbf{x}}_{\mathrm{p}}(\hat{t}_{\mathrm{CPA}}) - \mathbf{x}] \tag{53}$$

subject to

$$\|\mathbf{s}(\hat{t}_{\mathrm{CPA}}) - \mathbf{x}\| \leq \Delta d \tag{54}$$

5.2. Collision Warning Based on a Bayesian Approach

In the Bayesian approach instead of using $\hat{t}_{\mathrm{CPA}}$ as "the collision time," the approach accounts for t_{CPA} as a random variable. Since the CPA distance d_{CPA} (the distance between the target and the ownship at the CPA time) is a function of the CPA time, d_{CPA} is also a random variable. One can define the collision event based on d_{CPA} and estimate the probability of collision based on an estimated pdf of d_{CPA}.

1) CPA distance as a function of the target parameter:

Under the assumption that both the target and the ownship are moving with constant velocities, the CPA time is when the target and the ownship are closest to each other, that is

$$\begin{aligned}t_{\mathrm{CPA}} &= \arg\min_t \|\mathbf{x}_p(t) - \mathbf{s}(t)\| \\ &= \arg\min_t \|(\mathbf{x}_0 + t\dot{\mathbf{x}}_0) - (\mathbf{s}_0 + t\dot{\mathbf{s}}_0)\| \\ &= \arg\min_t \|(\mathbf{x}_0 + t\dot{\mathbf{x}}_0) - (\mathbf{s}_0 + t\dot{\mathbf{s}}_0)\|^2 \\ &= \arg\min_t d^2\end{aligned} \tag{55}$$

Taking the derivative of d^2 with respect to t and setting it to zero

$$\frac{dD}{dt} = 2[(\mathbf{x}_0 + t\dot{\mathbf{x}}_0) - (\mathbf{s}_0 + t\dot{\mathbf{s}}_0)]'[\dot{\mathbf{x}}_0 - \dot{\mathbf{s}}_0] = 0 \tag{56}$$

[2]This is a generalized likelihood function because it relies on $\hat{t}_{\mathrm{CPA}}$, which is an estimate.

the CPA time is obtained as

$$t_{\text{CPA}} = -\frac{[\mathbf{x}_0 - \mathbf{s}_0]'[\dot{\mathbf{x}}_0 - \dot{\mathbf{s}}_0]}{\|\dot{\mathbf{x}}_0 - \dot{\mathbf{s}}_0\|^2} \tag{57}$$

and the CPA distance is therefore a function of the target parameter $\mathbf{x}$ in (2)

$$\begin{aligned} d_{\text{CPA}} &= f(\mathbf{x}) = \|\mathbf{x}_p(t_{\text{CPA}}) - \mathbf{s}(t_{\text{CPA}})\| \\ &= \|\mathbf{x}_0 - \mathbf{s}_0 - \frac{[\mathbf{x}_0 - \mathbf{s}_0]'[\dot{\mathbf{x}}_0 - \dot{\mathbf{s}}_0]}{\|\dot{\mathbf{x}}_0 - \dot{\mathbf{s}}_0\|^2}(\dot{\mathbf{x}}_0 - \dot{\mathbf{s}}_0)\| \end{aligned} \tag{58}$$

In the above, $\|\cdot\|$ is the Cartesian norm.

2) Estimation of the probability density of d_{CPA}:

Assuming a diffuse (non-informative) prior density for the target parameter $\mathbf{x}$, as in [2], the posterior density of $\mathbf{x}$ conditioned on $\hat{\mathbf{x}}_{\text{ML}}$, given by (29), is approximated as

$$p[\mathbf{x} \mid \hat{\mathbf{x}}_{\text{ML}}] = \mathcal{N}[\mathbf{x}; \hat{\mathbf{x}}_{\text{ML}}, J^{-1}] \tag{59}$$

This Gaussian approximation is reasonable as Section 6 shows that the ML estimate can be considered as unbiased and statistically efficient, that is, (17) and (18) hold.

One possible way of estimating the density of d_{CPA} is to draw N_s samples of $\mathbf{x}$ from (59), obtain N_s samples of d_{CPA} and fit a density based on these samples. In this paper, we estimate the pdf of d_{CPA} as a Rician distribution. The validity of fitting the Rician distribution is confirmed in Section 6. The Rician distribution with noncentrality parameter $\nu \geq 0$ and scale parameter $\sigma > 0$ has the density function

$$p_{d_{\text{CPA}}}(x \mid \nu, \sigma) = \frac{x}{\sigma^2} \exp\left(-\frac{x^2 + \nu^2}{2\sigma^2}\right) I_0\left(\frac{x\nu}{\sigma^2}\right), \quad x > 0 \tag{60}$$

where $I_0(\cdot)$ is the zero-order modified Bessel function of the first kind. Based on the N_s samples of d_{CPA}, the ML estimates ν^{ML} and σ^{ML} can be obtained using the method presented in [12].

3) Decision making:

One can define the collision event as

$$\{\text{Collision}\} = \{d_{\text{CPA}} \leq d_{\min}\} \tag{61}$$

where $d_{\min}$ is the minimum distance between the aircraft for which a collision will not occur, that is, one believe that a collision occurs if the estimated d_{CPA} is less than $d_{\min}$ by taking the aircraft dimensions into account. Therefore, the probability of collision is

$$\begin{aligned} \text{P}_c &= \text{P}(\{\text{Collision}\}) = \text{P}(\{d_{\text{CPA}} \leq d_{\min}\}) \\ &= \int_0^{d_{\min}} p_{d_{\text{CPA}}}(x \mid \nu^{\text{ML}}, \sigma^{\text{ML}}) dx \end{aligned} \tag{62}$$

The integration in (62) is evaluated using the MATLAB function "cdf." The average computational time in a single run, including the target parameter estimation, sampling, Rician distribution parameter estimation and the integration (62), is around 0.6 s. This computation is performed in MATLAB 2015a on a Windows machine equipped with a 2.40 GHz Intel Core 2 Quad CPU with 4 GB RAM. Consequently, we feel it is not unreasonable to claim that it would be real-time feasible with a dedicated processor and code in machine language.

If P_c is smaller than, say, 0.0001%, the collision is unlikely and no warning will be issued. Otherwise, a warning will be given.

6. SIMULATION RESULTS

6.1. Efficiency of ML Estimator of the Target Parameter

Under the hypothesis $H_{\mathbf{x}}$ that the ML estimator (29) is unbiased and efficient, that is, the mean of the estimation error is zero and the estimation errors match the covariance given by the CRLB as in (18), the NEES for the target parameter

$$\epsilon_{\mathbf{x}} = \tilde{\mathbf{x}}' J \tilde{\mathbf{x}} \tag{63}$$

is chi-square distributed with $n_{\mathbf{x}}$ degrees of freedom. The sample average NEES from N Monte Carlo runs would be

$$\bar{\epsilon}_{\mathbf{x}} = \frac{1}{N} \sum_{i=1}^{N} \epsilon_{\mathbf{x}}^i \tag{64}$$

where $\epsilon_{\mathbf{x}}^i$ is a sample from ith Monte Carlo run. The quantity $N\bar{\epsilon}_{\mathbf{x}}$ is chi-square distributed with $Nn_{\mathbf{x}}$ degrees of freedom. Therefore, for a given level of significance α, $H_{\mathbf{x}}$ cannot be rejected if

$$\bar{\epsilon}_{\mathbf{x}} \in \left[\frac{L_{\mathbf{x}}}{N}, \frac{U_{\mathbf{x}}}{N}\right] \tag{65}$$

where $L_{\mathbf{x}}$ and $U_{\mathbf{x}}$ are the $100\alpha/2$ and $100(2-\alpha)/2$ percentile points of a chi-square random variable with $Nn_{\mathbf{x}}$ degrees of freedom.

The sample averages of the NEES for the 6-D target parameter ($n_{\mathbf{x}} = 6$) in Scenario 5 from 100 Monte Carlo runs based on the CRLB evaluated at the truth and at the estimate are calculated. The values are 6.2576 and 6.2207, which can be considered practically identical. Both values fall inside the two-sided 60% probability region [5.70, 6.29], which means that one can accept the null hypothesis $H_{\mathbf{x}}$ at a high significance level of 40%, i.e., we allow a probability of making a type I (reject $H_{\mathbf{x}}$ when it is true) error that is 40% in this case. In addition, the likelihood function (13) is exponential, which is a necessary, although not sufficient, condition for the MLE to be efficient [16]. This strongly affirms the acceptability of the CRLB as the actual covariance of the 3-D estimator in Scenario 5. The same reasoning was used in [11] to demonstrate the statistical efficiency of composite position measurements from passive sensors for a variety of geometries.

The sample averages of the NEES for the 4-D target parameter ($n_{\mathbf{x}} = 4$) in Scenario 9 from 100 Monte Carlo runs based on the CRLB evaluated at the truth and at the estimate are also calculated. The values are

3.9209 and 3.9199, which can also be considered practically identical. Both values fall inside the two-sided 30% probability region [3.885, 4.103] (i.e., the alternative hypothesis H_1 ("not efficient") is rejected at a rather high significance level of 70%), which confirms the acceptability of the CRLB as the actual covariance of the 2-D estimator in Scenario 9. Therefore, the unbiasedness and efficiency of the ML estimator is verified in both scenarios considered in this paper.

Simulation results also show that the collision warning algorithm based on the CRLB covariance provides reliable performance by comparing the CRLB-based error probability of 10^{-5} with 10^5 Monte Carlo runs. The number of missed collision detections in this case was 2 in 10^5 runs. If one considers the following hypothesis test

$$H_0 : P_{\text{FA}} = 10^{-5} \tag{66}$$

$$H_1 : P_{\text{FA}} > 10^{-5} \tag{67}$$

then, based on the Poisson approximation with parameter λ of the binomial distribution of the number of missed detections in 10^5 runs ($H_0 : \lambda = 1$; $H_1 : \lambda > 1$ with 10^5 runs), the probability of getting no more than 2 missed collision detections is 0.9197, i.e., we can accept H_0 at a level of significance of 8%. (The outcome is to the left of the 8% tail.) With 10^5 runs and the threshold set for $P_{\text{FA}} = 10^{-4}$ (then $H_0 : \lambda = 10$), we obtained 5 missed collision detections, i.e., in this case H_0 can be accepted at a level of significance of 93% (unusually high).

6.2. Efficiency of the CPA Time Estimate

Based on (36), the CPA time estimate $\hat{t}_{\text{CPA}}$ in (37) is a function of the target parameter estimate $\hat{\mathbf{x}}$, denoted as

$$\hat{t}_{\text{CPA}} = g[\hat{\mathbf{x}}] \tag{68}$$

Unfortunately, the function g has no closed-form expression, therefore, we estimate the variance of $\hat{t}_{\text{CPA}}$ using the unscented transformation technique [3] as follows:

Firstly, by the method of moment matching, the Gaussian density $\mathcal{N}(\hat{\mathbf{x}}; \mathbf{x}_{\text{t}}, P)$ of the $n_{\mathbf{x}}$-dimensional $\hat{\mathbf{x}}$ (centered at the true value $\mathbf{x}_{\text{t}}$; this is in view of the unbiasedness and efficiency discussed in the previous subsection) is replaced by a $(2n_{\mathbf{x}}+1)$-point probability mass function (pmf)

$$p(\hat{\mathbf{x}}) = \sum_{i=-n_{\mathbf{x}}}^{n_{\mathbf{x}}} w^i \delta(\hat{\mathbf{x}} - \hat{\mathbf{x}}^i) \tag{69}$$

where $\delta(\cdot)$ is the Dirac delta function. The sigma points of the pmf are

$$\hat{\mathbf{x}}^i = \mathbf{x}_{\text{t}} + \text{sgn}(i) a [P]^{1/2}_{|i|} \quad i = -n_{\mathbf{x}}, \ldots, n_{\mathbf{x}}; \quad a \in \mathbb{R} \tag{70}$$

where $[P]_i^{1/2}$ is the ith column of the Cholesky factor of P defined by

$$\sum_{i=1}^{n_{\mathbf{x}}} [P]_i^{1/2} ([P]_i^{1/2})' = P \tag{71}$$

and the signum function is defined as

$$\text{sgn}(i) \stackrel{\Delta}{=} \begin{cases} -1 & i < 0 \\ 0 & i = 0 \\ 1 & i > 0 \end{cases} \tag{72}$$

The point masses are [3]

$$w^i = \begin{cases} \dfrac{1}{2a^2} & |i| = 1, \ldots, n_{\mathbf{x}} \\ \dfrac{a^2 - n_{\mathbf{x}}}{a^2} & i = 0 \end{cases} \tag{73}$$

which sum up to unity. With the sigma points and point masses specified above, the pmf (69) has the same mean and covariance matrix as the Gaussian pdf $\mathcal{N}(\hat{\mathbf{x}}; \mathbf{x}_{\text{t}}, P)$ regardless of the value of a. A reasonable choice of a is $\sqrt{n_{\mathbf{x}} + 2}$, so we use that in this paper. In a simulated scenario, the true value of the parameter is known. However, in a real scenario where the true value of the parameter is unknown and needs to be estimated, the sigma points of $\hat{\mathbf{x}}$ need to match the moments of $\mathcal{N}(\hat{\mathbf{x}}, P)$ with P evaluated at the estimate.

Secondly, a sigma point of $\hat{t}_{\text{CPA}}$ corresponding to $\hat{\mathbf{x}}^i$ can be obtained as

$$\hat{t}^i = g[\hat{\mathbf{x}}^i] \tag{74}$$

Lastly, the pdf of $\hat{t}_{\text{CPA}}$ is approximated by the pmf

$$p(\hat{t}_{\text{CPA}}) = \sum_{i=-n_{\mathbf{x}}}^{n_{\mathbf{x}}} w^i \delta(\hat{t}_{\text{CPA}} - \hat{t}^i) \tag{75}$$

which has mean

$$\bar{t} = \sum_{i=-n_{\mathbf{x}}}^{n_{\mathbf{x}}} w^i \hat{t}^i \tag{76}$$

and variance

$$\sigma_t^2 = \sum_{i=-n_{\mathbf{x}}}^{n_{\mathbf{x}}} w^i (\hat{t}_i - \bar{t})^2 \tag{77}$$

If we assume that $\hat{t}_{\text{CPA}}$ is a Gaussian random variable with mean t_{CPA} and variance σ_t^2, then under the hypothesis H_t that the estimator (37) is unbiased and efficient, the NEES for the CPA time

$$\epsilon_t = \frac{(t_{\text{CPA}} - \hat{t}_{\text{CPA}})^2}{\sigma_t^2} \tag{78}$$

is chi-square distributed with 1 degree of freedom. The sample average NEES from N Monte Carlo runs would be

$$\bar{\epsilon}_t = \frac{1}{N} \sum_{i=1}^{N} \epsilon_t^i \tag{79}$$

where ϵ_t^i is a sample from ith Monte Carlo run. The quantity $N\bar{\epsilon}_t$ is chi-square distributed with N degrees of

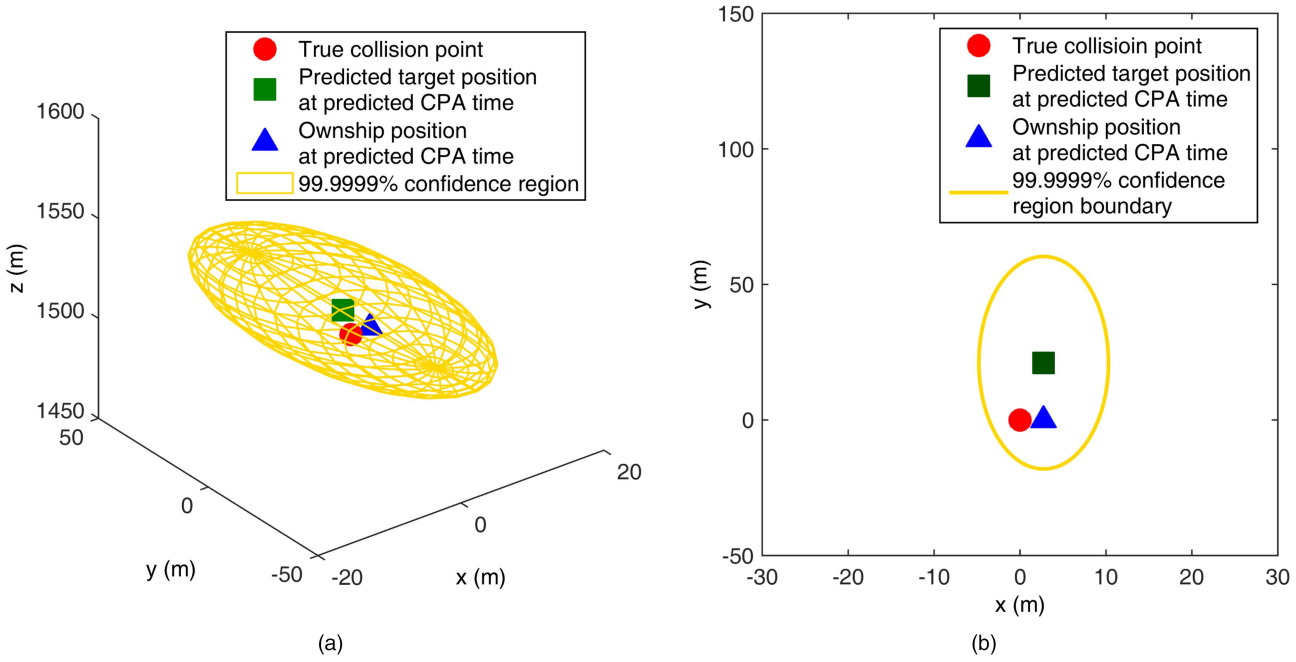

Fig. 6. Collision warning is "on" in a single run in Scenarios 5 and 9. (a) Scenario 5. (b) Scenario 9.

freedom. Therefore, for a given level of significance α, H_t cannot be rejected if

$$\bar{\epsilon}_t \in \left[\frac{L_t}{N}, \frac{U_t}{N}\right] \tag{80}$$

where L_t and U_t are the $100\alpha/2$ and $100(2-\alpha)/2$ percentile points of a chi-square random variable with N degrees of freedom.

The sample averages of the NEES for the CPA time estimate in Scenario 5 from 100 Monte Carlo runs based on the true value and the estimate of the target parameter are calculated. The values are 1.0914 and 1.0950, which can be considered practically identical. Both values fall inside the two-sided 60% probability region [0.879, 1.117], which confirms the unbiasedness and efficiency of the CPA time estimate in Scenario 5 for the 3-D case. The sample averages of the NEES for the CPA time estimate in Scenario 9 from 100 Monte Carlo runs based on the true value and the estimate of the target parameter are calculated. The values are 0.8753 and 0.8737, which can also be considered practically identical. Both values fall inside the two-sided 60% probability region, which confirms the unbiasedness and efficiency of the CPA time estimate in Scenario 9 for the 2-D case.

6.3. Collision Warning Based on the Generalized Likelihood Function

The collision warning is "on" for all 100 runs in Scenario 5 and 9 with the target and the ownship modeled as points, that is, at the predicted CPA time the ownship is inside the confidence region of the true target around its predicted position as illustrated in Figure 6(a) and 6(b). The collision warning is "off" for all 100 runs in Scenario 6, that is, at the predicted CPA time the ownship is outside the confidence region of the true target around its predicted position as illustrated in Figure 7(a).

Taking the physical dimensions of the aircraft into consideration and using a safety margin of 100 m, the collision warning is "on" for all 100 runs in Scenario 5 and 9. However, the collision warning is "on" for all 100 runs in Scenario 6, that is, false alarms occur. Although at the predicted CPA time the ownship is outside the confidence region of the true target around its predicted position, the minimum distance between the ownship and the ellipsoid is less than the safety margin as illustrated in Figure 7(b).

The term "CPA angle" is defined as the angle formed by the target velocity vector and the ownship velocity vector at the CPA time when they are projected on a plane at the same altitude. Therefore, the CPA angle is 180° in Scenarios 5, 6 and 9.

The performance of the 3-D likelihood-based collision warning algorithm is further evaluated by varying the target and ownship altitude separation[3] from 0 to 300 m in steps of 50 m and the CPA angle from 180° to 135° in steps of 15° one parameter at a time in Scenario 5. From Figure 8(a), the 3-D likelihood based collision warning algorithm has no missed detections of a collision in 100 runs. There are some false alarms when the intruder and ownship altitude separation is 50 m and the number of false alarms increases slightly with the CPA angle decreasing. There are no false alarms when the intruder and ownship altitude separation is beyond 100 m.

[3] 1000 ft (≈ 300 m) is a global standard for vertical separation

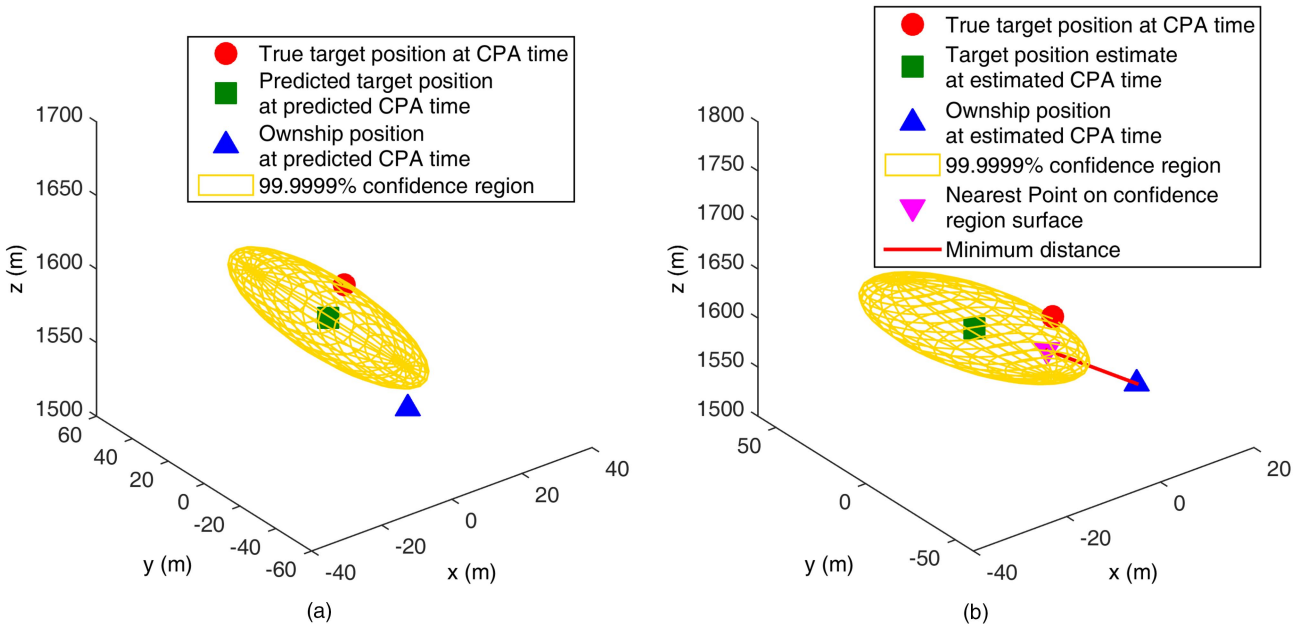

Fig. 7. Collision warning decisions in a single run in Scenario 6. Collision warning is "off" without a safety margin but is "on" with a safety margin of 100 m. (a) Without a safety margin. (b) With a safety margin of 100 m.

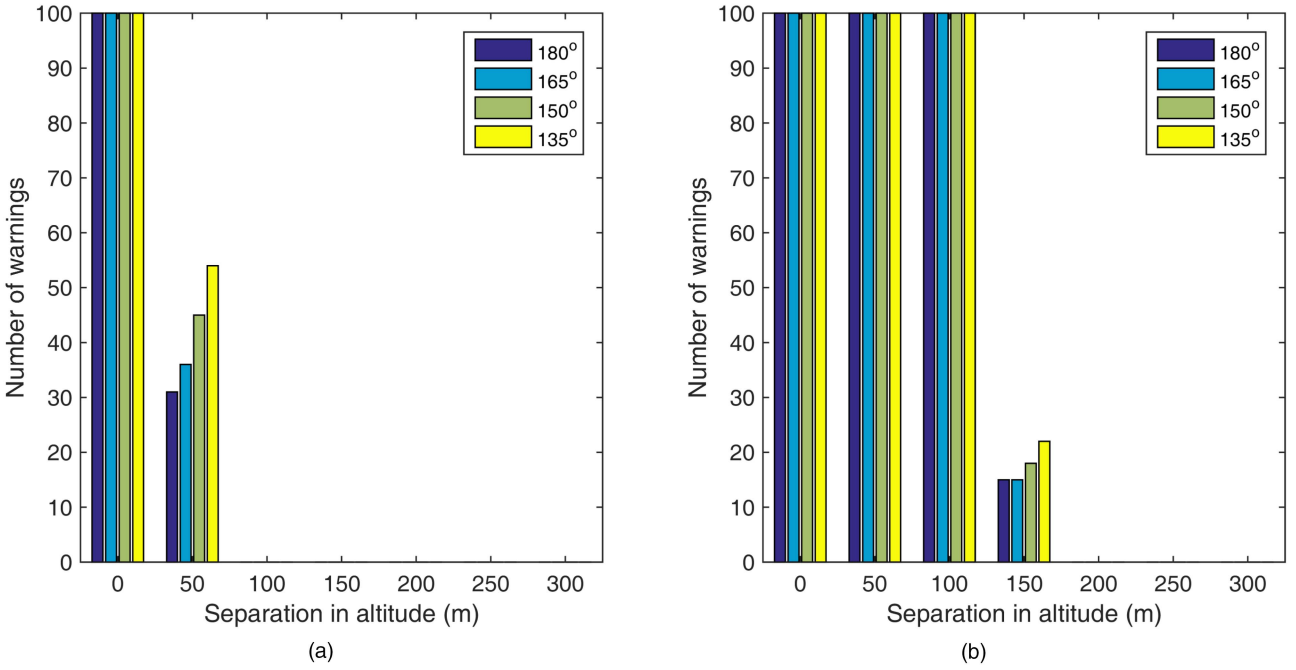

Fig. 8. The number of warnings in 100 runs using the 3-D likelihood based collision warning algorithm. (a) Without a safety margin. (b) With a safety margin of 100 m.

Figure 9(a) shows the histogram of the logarithm of the estimated probability of collision in 10, 000 runs from scenarios with different CPA angles when there is a collision (the target and ownship altitude separation is 0 m). The estimated probability of collision has a similar distribution for different CPA angles, which is also observed at other levels of altitude separation. More than 95% of the time, the probability of collision is estimated to be larger than 10%. Since the probability of collision is always estimated to be larger than 0.0001%, there are no missed detections, which confirms the results shown in Figure 8(a). As the separation in altitude increases from 0 to 50 m, the estimated probability of collision gets much smaller as shown in Figure 9(b). Similar phenomena are also observed at other CPA angles. False alarms occur about 30% of the time when the estimated probability of collision is larger than 0.0001%. When the intruder and ownship altitude separation is beyond 100 m, the estimated probability is always less than 10^{-16} and hence

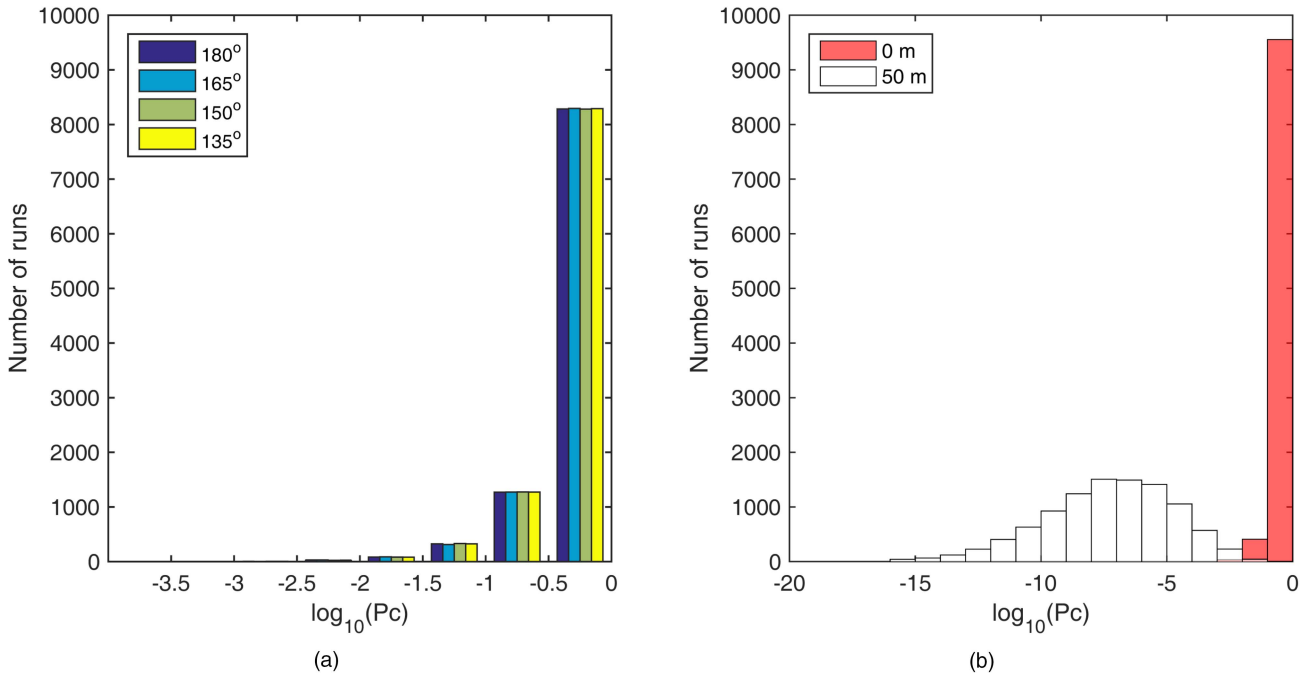

Fig. 9. The histogram of $\log_{10} P_c$ in 10000 runs using the 3-D likelihood based collision warning algorithm. (a) Separation in altitude is 0 m. (b) CPA angle is 180°.

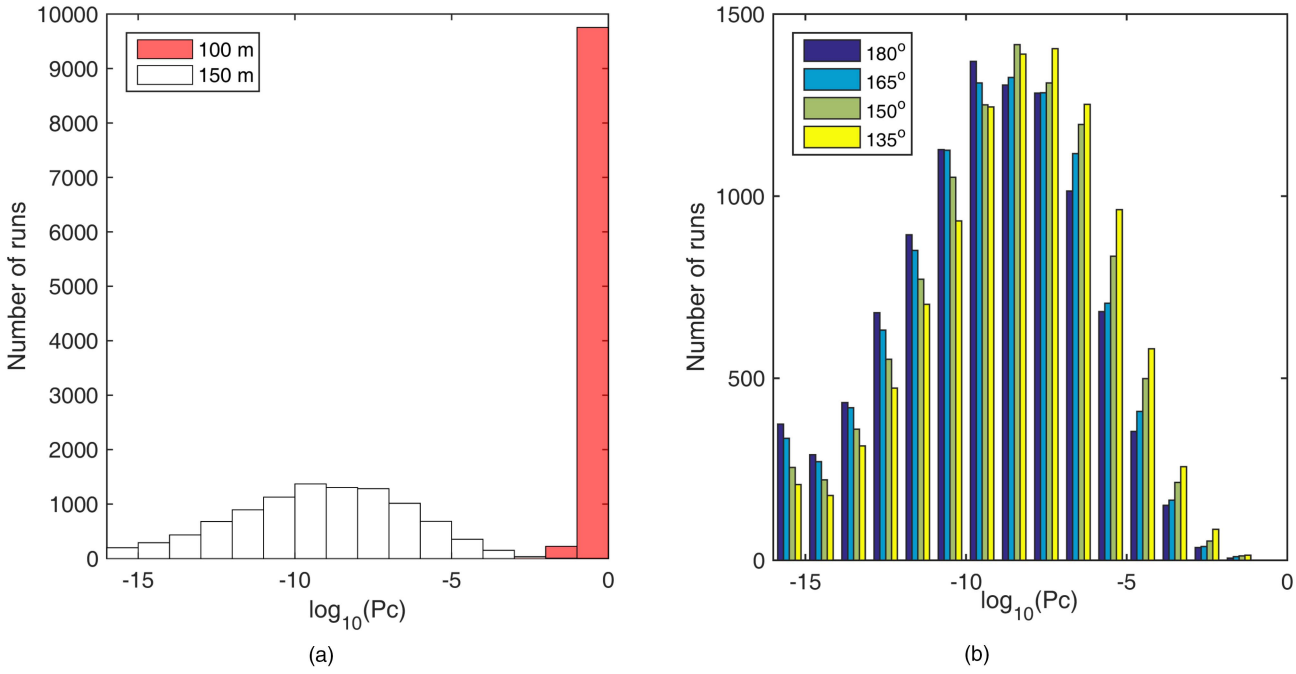

Fig. 10. The histogram of $\log_{10} P_c$ in 10000 runs using the 3-D likelihood based collision warning algorithm with a safety margin of 100 m. (a) CPA angle is 180°. (b) Separation in altitude is 150 m.

the corresponding distributions are not shown in Figure 9(b).

With a safety margin of 100 m, from Figure 8(b), the 3-D likelihood based collision warning algorithm has no missed detections of a collision. However, it becomes more conservative and there are always false alarms when the intruder and ownship altitude separation is below 100 m, which is not surprising because of a safety margin of same distance. The number of false alarms starts to decrease at 150 m altitude separation.

When the altitude separation is 0 or 50 m, it turns out that the estimated probability of collision is always 1 in 10,000 Monte Carlo runs. When the altitude separation is 100 m, the estimated probability of collision is not always unity: see Figure 10(a) for the distribution of its logarithm. When the separation is 150 m, the estimated

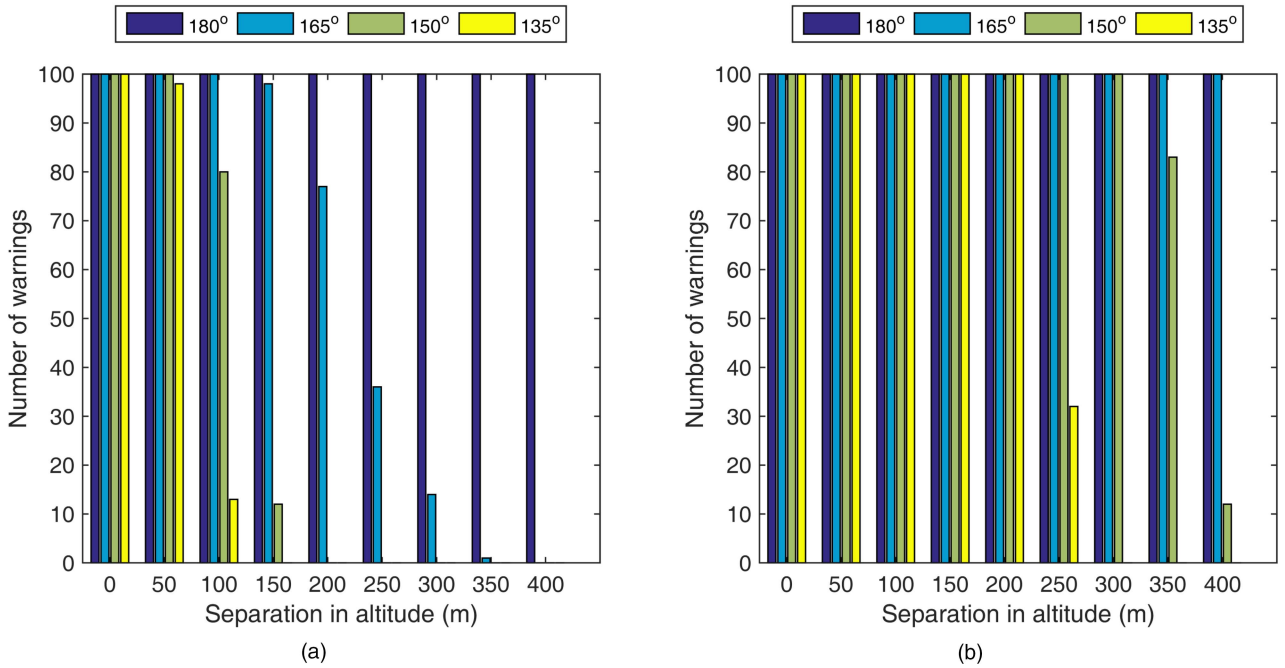

Fig. 11. The number of warnings in 100 runs using the 2-D likelihood based collision warning algorithm. (a) Without a safety margin. (b) With a safety margin of 100 m.

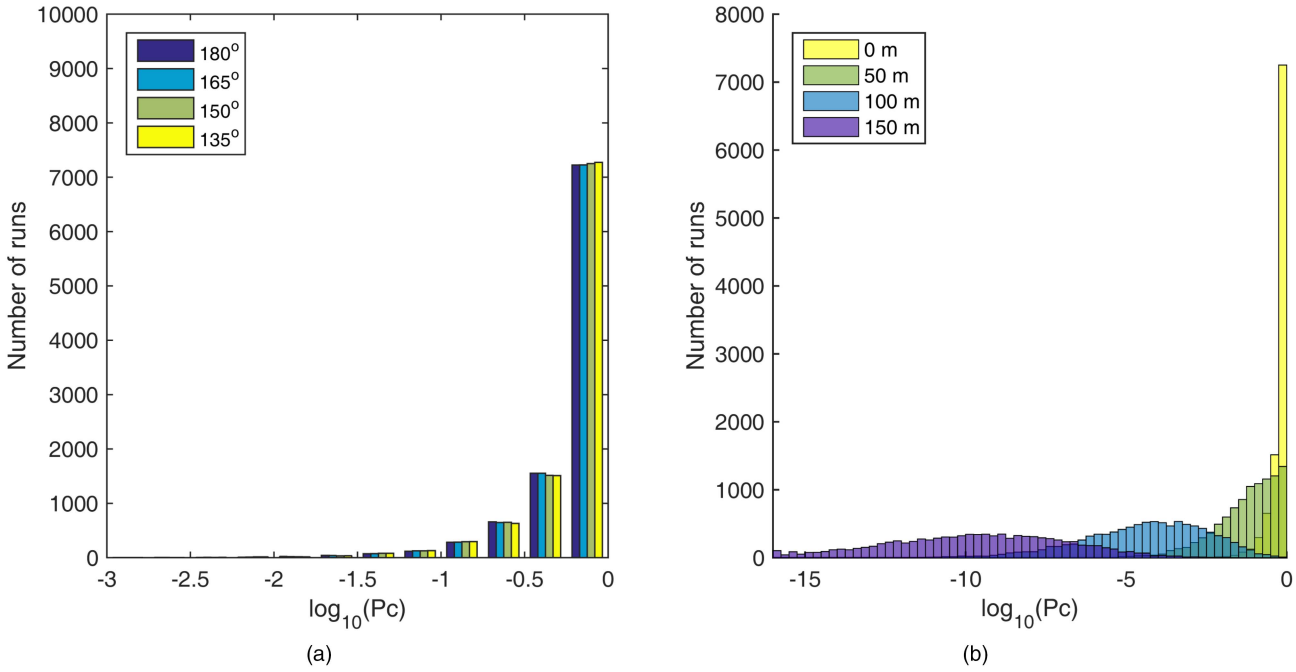

Fig. 12. The histogram of $\log_{10} P_c$ in 10000 runs using the 2-D likelihood based collision warning algorithm. (a) Separation in altitude is 0 m. (b) CPA angle is 150°.

probability of collision becomes much smaller. The similar distributions are also observed at other CPA angles as illustrated in Figure 10(b). It is estimated to be less than 0.0001% for more than 90% of the time. When the intruder and ownship altitude separation is beyond 200 m, the estimated probability is always less than 10^{-16}.

The performance of the 2-D likelihood based collision warning algorithm is evaluated in the same manner. Figure 11(a) shows that there are no missed detections of collisions in 100 runs, which is the same as in the 3-D scenarios. The estimated probability of collision is very close to 1 for most of the time in 10000 runs and its distribution is similar at different CPA angles as indi-

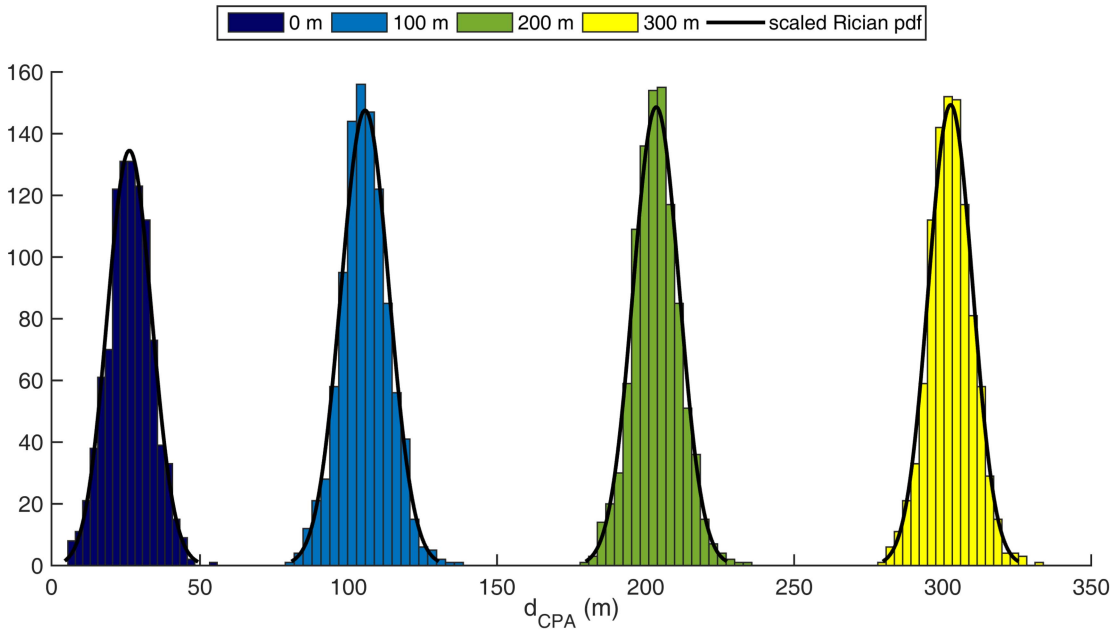

Fig. 13. The histograms of d_{CPA} with fitted Rician distributions when the CPA angle is 180°.

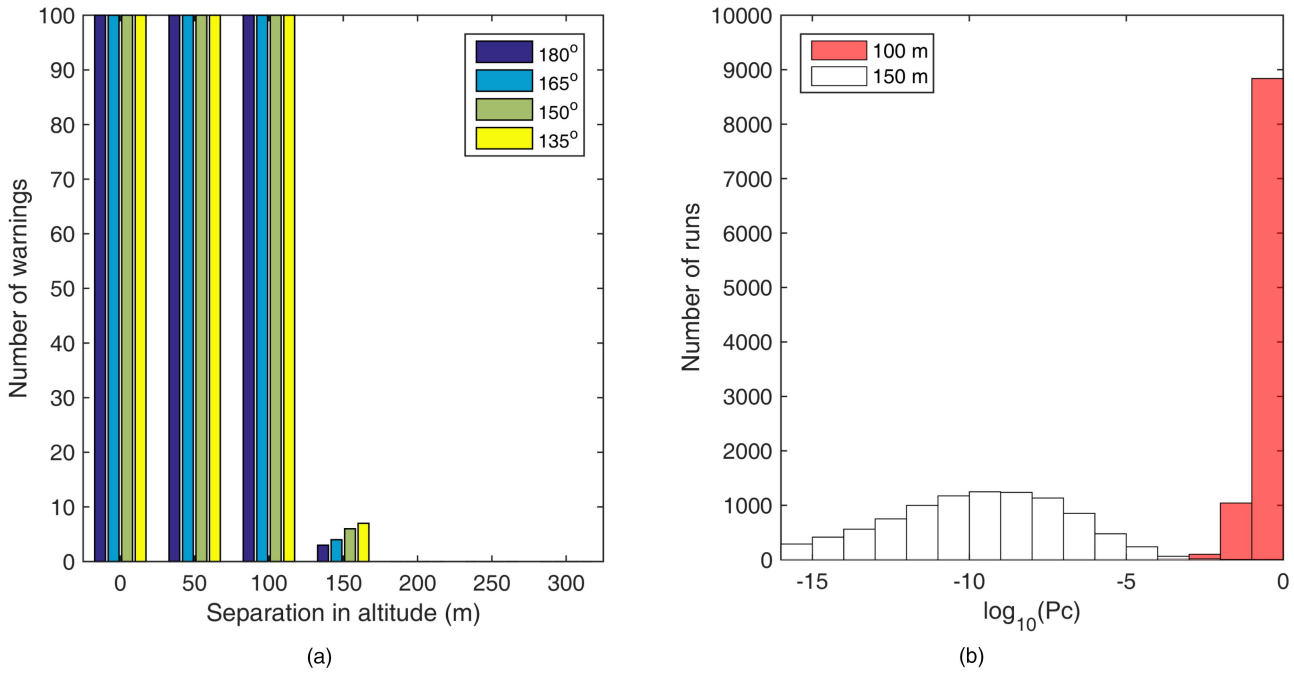

Fig. 14. Performance of the 3-D Bayesian collision warning algorithm with d_{min} = 100 m. (a) Histogram of the number of warnings in 100 runs. (b) Histogram of $\log_{10} \mathrm{P}_c$ in 10000 runs with CPA angle 180°.

cated in Figure 12(a). The CPA angle has a pronounced effect on false alarms in the 2-D case. Recall that in the 2-D scenarios it is (conservatively) assumed that the intruder is at the same altitude as the ownship, which is not true when the altitude separation is not zero. When the CPA angle is close to 180°, the collision is very likely to occur based on the same altitude assumption, and, consequently, the false alarm rate is therefore very high. At other CPA angles, as the altitude separation increases, the number of false alarms decreases and the estimated probability of collision becomes smaller as indicated in Figure 12(b).

With a safety margin of 100 m, there are no missed detections of collisions. However, there are more false alarms because of both the same altitude assumption and the safety margin.

Based on the above observations, we submit that 3-D estimation with at least 3 transmitters is the only one reliable configuration for collision warning and that 2-D estimation with 2 transmitters is prone to false alarms

when the CPA angle is 180° even if there is more than 400 m altitude separation.

6.4. Collision Warning Based on the Bayesian Approach

The one-sample Kolmogorov-Smirnov test fails to reject the hypothesis that 1000 samples of d_{CPA} comes from a Rician distribution with parameters that are ML estimates based on the same 1000 samples in all 100 Monte Carlo runs in each of the 3-D scenarios that are used to evaluate the likelihood based collision warning algorithm in previous subsection. The fitted Rician distributions with the corresponding histograms of d_{CPA} at different levels of altitude separations at 180° CPA angle are shown in Figure 13. As shown in the previous subsection, 2-D collision warning with 2 transmitters under the same altitude assumption is unreliable because it is prone to false alarm, therefore the Bayesian approach is considered only in the multistatic configuration with 3 transmitters in this paper. It turned out that the hypothesis that the pdf of d_{CPA} is Rician is no longer valid in the 2D scenarios when the same altitude assumption does not hold. Nevertheless, it is possible to estimate the probability of collision by fitting a kernel distribution instead of a Rician distribution in those 2-D scenarios.

The performance of 3-D Bayesian collision warning algorithm with $d_{\min} = 100$ m is shown in Figure 14, which is very similar to that of 3-D likelihood based collision warning algorithm with a safety margin 100 m. There are no missed detections of a collision but there are always false alarms when the intruder and ownship altitude separation is below 100 m. The number of false alarms starts to decrease at 150 m altitude separation and becomes zero when the altitude separation is beyond 200 m.

Comparing Figure 14(b) and 10(a), the estimated probability of collision from the 3-D Bayesian algorithm has a similar distribution to that from the 3-D likelihood based algorithm. As the altitude separation increases, the estimated probability of collision is getting smaller. When the altitude separation is 0 or 50 m, it turns out the estimated probability of collision is always 1 in 10,000 Monte Carlo runs. When the intruder and ownship altitude separation is beyond 200 m, the estimated probability is always less than 10^{-16}.

7. CONCLUSIONS

The ability to sense and avoid non-cooperative targets is essential for UAS to perform routine tasks when they are not alone in the airspace. We investigated several configurations with bistatic range and range rate measurements for collision warning. It turned out that a multistatic configuration is needed to provide good observability of the target, which is useful for collision warning. The minimum number of the transmitters required is three in a 3-D scenario and two in a 2-D scenario. We also implemented an ML estimator in both types of scenarios using the ILS technique and showed that the estimator can be considered as statistically efficient through Monte Carlo simulations for the scenarios considered. Based on the ML estimator, the collision warning was approached in two different ways. The first method is formulating the collision as a hypothesis testing problem using a generalized likelihood function, where the efficiency of the CPA time is also verified. The second method is a Bayesian formulation focusing on the time of CPA modeled as a random variable. Only the multistatic configuration with three transmitters is reliable for collision warning because the multistatic configuration with two transmitters based on the same target and ownship altitude assumption turns out to be prone to false alarms. When the minimum distance in the Bayesian approach is the same as the safety margin in the likelihood based approach, both algorithms yield very similar collision warning performance.

ACKNOWLEDGEMENT

Stimulating discussions with Melissa Meyer and Robert Coury are gratefully acknowledged. This work is supported by ARO W991NF-10-1-0369.

REFERENCES

[1] B. M. Albaker, and N. A. Rahim
A survey of collision avoidance approaches for unmanned aerial vehicles.
In *International Conference for Technical Postgraduates*, Dec. 2009.

[2] Y. Bar-Shalom, X.-R. Li, and T. Kirubarajan
Estimation with Applications to Tracking and Navigation: Theory, Algorithms and Software.
New York: Wiley, 2001.

[3] Y. Bar-Shalom, P. K. Willett, and X. Tian
Tracking and Data Fusion: A Handbook of Algorithms.
Storrs, CT: YBS Publishing, 2011.

[4] S. S. Blackman, and R. Popoli
Design and Analysis of Modern Tracking Systems.
Artech House, 1999.

[5] C. Carbone, U. Ciniglio, F. Corraro, and S. Luongo
A novel 3D geometric algorithm for aircraft autonomous collision avoidance.
In *Proceedings of 45th IEEE Conference on Decision and Control*, Dec. 2006, 1580–1585.

[6] B. K. Chalise, Y. D. Zhang, M. G. Amin, and B. Himed
Target localization in a multi-static passive radar system through convex optimization.
Signal Processing, 102, 0 (2014), 207–215.

[7] W. Dou, P. K. Willett, and Y. Bar-Shalom
Fusion of range-only measurements from multistatic configurations for air collision warning.
In *Proceedings of IEEE Aerospace Conference*, March 2015.

[8] W. Dou, P. K. Willett, and Y. Bar-Shalom
Configuration selection for fusion of measurements from multistatic radars for air collision warning.
In *Proceedings of 18th International Conference on Information Fusion*, July 2015.

[9] Y. K. Kwag, and C. H. Chung
UAV based collision avoidance radar sensor.
In *IEEE International Geoscience and Remote Sensing Symposium*, July 2007, 639–642.

[10] M. Malanowski, and K. Kulpa
Two methods for target localization in multistatic passive radar.
IEEE Transactions on Aerospace and Electronic Systems, 48, 1 (Jan. 2012), 572–580.

[11] R. W. Osborne, III and Y. Bar-Shalom
Statistical efficiency of composite position measurements from passive sensors.
IEEE Transactions on Aerospace and Electronic Systems, 49, 4 (Oct. 2013), 2799–2806.

[12] J. Sijbers, A. J. den Dekker, P. Scheunders, D. Van Dyck
Maximum-likelihood estimation of Rician distribution parameters.
IEEE Transactions on Medical Imaging, 17, 3 (June 1998), 357–361.

[13] D. Sislak, M. Rehak, M. Pechoucek, D. Pavilicek and M. Uller
Negotiation-based approach to unmanned aerial vehicles.
In *IEEE 2006 Workshop on Distributed Intelligent Systems*, June 2006, 279–284.

[14] M. Švecová, D. Kocur, R. Zetik, and J. Rovňáková,
Target localization by a multistatic UWB radar.
In *Proceedings of 20th International Conference Radioelektronika*, April 2010.

[15] C. J. Tomlin, J. Lygeros, and S. S. Sastry
A game theoretic approach to controller design for hybrid systems.
Proceedings of the IEEE, 88, 7 (July 2000), 949–970.

[16] H. L. Van Trees, K. L. Bell, and Z. Tian
Detection Estimation and Modulation Theory, 2nd Edition, Part I, Detection, Estimation, and Filtering Theory.
New York: Wiley, 2013.

[17] J.-H. Wen, J.-S. Li, C.-Y. Yang, C.-H. Chen, and H.-C. Chen
Localization scheme of multistatic radars system based on the information of measured signal.
In *Proceedings of 9th International Conference on Broadband and Wireless Computing, Communication and Applications*, Nov. 2014, 462–466.

[18] P. R. Williams
Aircraft collision avoidance using statistical decision theory.
In *Proceedings of SPIE 1694, Sensors and Sensor Systems for Guidance and Navigation II*, July 1992.

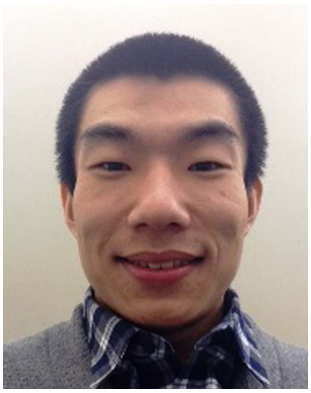

Wenbo Dou is a graduate student in the Department of Electrical and Computer Engineering at the University of Connecticut. He received the Bachelor of Engineering in Electrical and Electronic Engineering with First Class Honors from Nanyang Technological University in 2011. His current research interests are bias estimation, acoustic signal based multi-target localization and tracking, data fusion and machine learning.

Yaakov Bar-Shalom was born on May 11, 1941. He received the B.S. and M.S. degrees from the Technion, Israel Institute of Technology, in 1963 and 1967 and the Ph.D. degree from Princeton University in 1970, all in electrical engineering. From 1970 to 1976 he was with Systems Control, Inc., Palo Alto, California. Currently he is Board of Trustees Distinguished Professor in the Dept. of Electrical and Computer Engineering and Marianne E. Klewin Professor in Engineering at the University of Connecticut. He is also Director of the ESP (Estimation and Signal Processing) Lab. His current research interests are in estimation theory, target tracking and data fusion. He has published over 500 papers and book chapters in these areas and in stochastic adaptive control. He coauthored the monograph *Tracking and Data Association* (Academic Press, 1988), the graduate texts *Estimation and Tracking: Principles, Techniques and Software* (Artech House, 1993; translated into Russian, MGTU Bauman, Moscow, Russia, 2011), *Estimation with Applications to Tracking and Navigation: Algorithms and Software for Information Extraction* (Wiley, 2001), the advanced graduate texts *Multitarget-Multisensor Tracking: Principles and Techniques* (YBS Publishing, 1995), *Tracking and Data Fusion* (YBS Publishing, 2011),and edited the books *Multitarget-Multisensor Tracking: Applications and Advances* (Artech House, Vol. I, 1990; Vol. II, 1992; Vol. III, 2000). He has been elected Fellow of IEEE for "contributions to the theory of stochastic systems and of multi-target tracking." He has been consulting to numerous companies and government agencies, and originated the series of Multitarget-Multisensor Tracking short courses offered via UCLA Extension, at Government Laboratories, private companies and overseas. During 1976 and 1977 he served as Associate Editor of the *IEEE Transactions on Automatic Control* and from 1978 to 1981 as Associate Editor of *Automatica*. He was Program Chairman of the 1982 American Control Conference, General Chairman of the 1985 ACC, and Co-Chairman of the 1989 IEEE International Conference on Control and Applications. During 1983–87 he served as Chairman of the Conference Activities Board of the IEEE Control Systems Society and during 1987–89 was a member of the Board of Governors of the IEEE CSS. He was a member of the Board of Directors of the International Society of Information Fusion (1999–2004) and served as General Chairman of FUSION 2000, President of ISIF in 2000 and 2002 and Vice President for Publications in 2004–13. In 1987 he received the IEEE CSS Distinguished Member Award. Since 1995 he is a Distinguished Lecturer of the IEEE AESS and has given numerous keynote addresses at major national and international conferences. He is co-recipient of the M. Barry Carlton Award for the best paper in the *IEEE Transactions on Aerospace and Electronic Systems* in 1995 and 2000 and recipient of the 1998 University of Connecticut AAUP Excellence Award for Research. In 2002 he received the J. Mignona Data Fusion Award from the DoD JDL Data Fusion Group. He is a member of the Connecticut Academy of Science and Engineering. In 2008 he was awarded the IEEE Dennis J. Picard Medal for Radar Technologies and Applications, and in 2012 the Connecticut Medal of Technology. He has been listed by academic.research.microsoft (top authors in engineering) as #1 among the researchers in Aerospace Engineering based on the citations of his work.

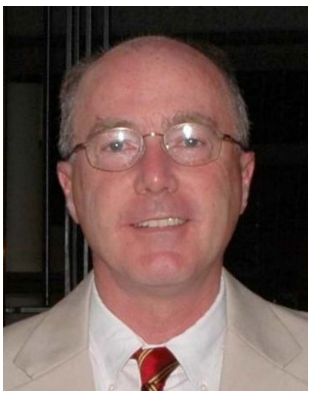

Peter Willett has been a faculty member in the Electrical and Computer Engineering Department at the University of Connecticut since 1986. Since 1998 he has been a Professor, and since 2003 an IEEE Fellow. His primary areas of research have been statistical signal processing, detection, machine learning, communications, data fusion, and tracking. He is editor-in-chief of *IEEE Signal Processing Letters*, 2014–2016. He was editor-in-chief for *IEEE Transactions on Aerospace and Electronic Systems* from 2006–2011, and AESS Vice President for Publications 2012–2014. He was associate editor for *IEEE Transactions on Aerospace and Electronic Systems* (for Data Fusion and Target Tracking), ISIF's *Journal of Advances in Information Fusion* and *IEEE Transactions on Systems, Man, and Cybernetics* (A and B). He is remains associate editor-in-chief for the IEEE AES Magazine. He is a member of the IEEE AESS Board of Governors and of the IEEE Signal Processing Society's Sensor-Array and Multichannel (SAM) technical committee (and is now Chair).